MSUCP-24

MICHIGAN STATE UNIVERSITY

CYCLOTRON PROJECT

Precise Methods for Pre-Calculation of Cyclotron Control Settings*

R. E. Berg

September 1966

Department of Physics

East Lansing, Michigan

ABSTRACT

PRECISE METHODS FOR PRE-CALCULATION
OF CYCLOTRON CONTROL SETTINGS

by Richard Eugene Berg

A computer program, SETOP, has been written which uses measured magnetic fields and a pre-computed set of ideal average fields to determine "operating points" for the MSU variable-energy, multi-particle cyclotron; to obtain a complete set of operating instructions, the experimenter need only specify the particle and energy of interest. Control settings are computed in a straightforward sequence of operations: (1) the fields at the desired excitation are synthesized by interpolation in the measured field data, (2) an average field is obtained using a modified least squares fit of the desired average field by the trim coils, and (3) the RF frequency is determined so as to minimize the energy spread of the beam in a single turn at the extraction energy. Independent numerical orbit studies were employed to investigate important features of the separated longitudinal equations of motion as used in SETOP, and several diagnostic procedures were investigated using numerical orbit integration to establish their validity under conditions obtained in the MSU cyclotron. Finally, the results of experimental measurements of several dynamical beam properties are presented which are in excellent agreement with pre-computed values.

ACKNOWLEDGMENTS

I should like to thank Dr. H. G. Blosser and Dr. M. M. Gordon for their guidance during this work. I am also grateful to T. I. Arnette, W. Joho, and D. A. Johnson for use of their computer programs in various phases of the numerical work.

A special word of thanks is also due Mr. Craig Barrows and Mrs. Judy Hilbert for their help in preparing the figures, and to Miss Wilma Sanders for her typing.

Finally, I am indebted to the National Science Foundation for the financial support without which this work would not have been possible—especially for an NSF Graduate Fellowship during the final year.

LIST OF TABLES

Figure Page

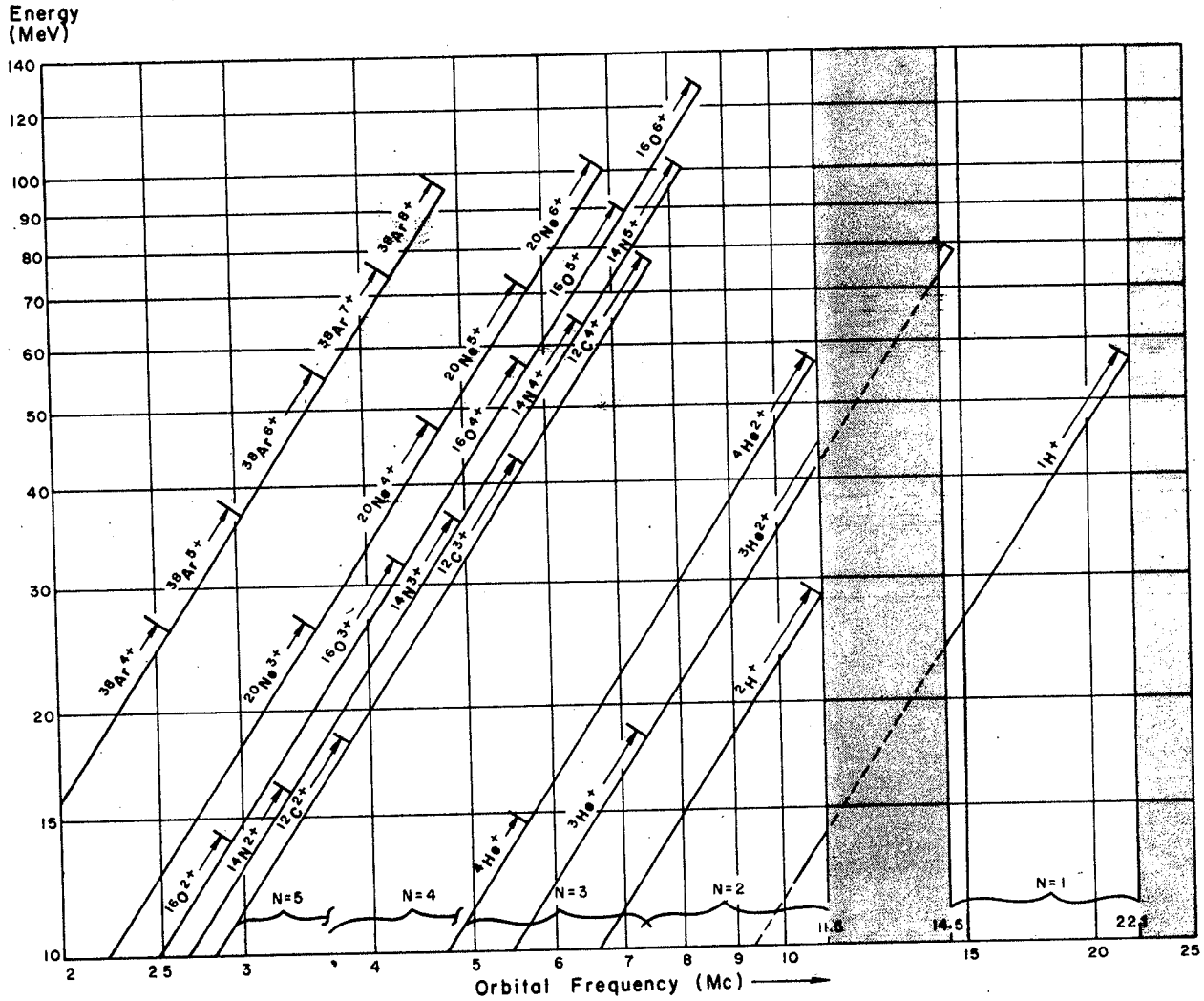

Figure 1. Energy versus orbital frequency for various particles which can be accelerated by the MSU cyclotron. Gray bands indicate areas outside the tuning range of the rf system; intermediate energy protons are obtained by using negative hydrogen ion acceleration with stripping extraction at partial radius.

possible within the limits of accuracy of the necessary measurements, where the best beam is defined as that with minimum energy spread at extraction possessing adequate optical properties. Computations predicting operating points for variable-energy cyclotrons have been performed previously, most notably those using a linear programming method through which trim coils, main field, and RF frequency and voltage may be simultaneously adjusted subject to constraints on various beam parameters such as axial and radial focusing frequencies and the phase of the particle with respect to the RF voltage[10]. This work deals with computation of cyclotron operating points for a multi-particle, variable-energy cyclotron such as the Michigan State University machine.

Preliminary to the final computations of operating conditions, an extensive set of magnetic field measurements was performed. A single computer program has been compiled which uses the measured magnetic field data and pre-computed ideal average fields to obtain operating points in a straightforward sequence of operations. Behavior of orbits in fields computed by the operating point program has been investigated theoretically with independent orbit integration programs, and the results of the two methods of computation are in good agreement. Results of a number of such studies are presented herein. Finally, beam dynamical properties have been experimentally measured and are found to be in excellent agreement with the computed values.

The approach toward computation of cyclotron operating points used at MSU is substantially different from the previous

quirements is a double three-point Lagrangian interpolation with provision for a weighting factor which forces continuity of the first derivative of the magnetic field with respect to main magnet excitation.

Linear orbit properties of the fitted magnetic fields are investigated by computing sets of equilibrium orbits (using the MSU equilibrium orbit program) covering the entire energy range for that field. Inspection of the equilibrium orbit data reflects the adequacy of the interpolation and field fitting procedures in terms of the requirements on the radial and axial focusing frequencies and the phase history. Typical results are presented in Section 7. The extraction energy, obtained from the equilibrium orbit data, is defined by the geometry of the magnetic field in the edge region and the position of the entrance to the electrostatic deflector. With the energy set the dee voltage is fixed to yield a uniform 220 turn orbit geometry for all particles at all extraction energies.

Finally, using decoupled longitudinal equations of motion, an RF frequency correction is computed which minimizes the energy spread of the beam at the extraction energy. This procedure is quite similar to the more familiar computation of a frequency which balances the phase history curve about zero degrees[12], but has the advantage of more precisely minimizing the energy spread of the extracted beam. Also, for comparison with other calculations, the longitudinal equations of motion are integrated to obtain the phase-energy history of the beam as a function of turn number.

Detailed discussion of methods and procedures outlined

I. MAGNETIC FIELD MEASUREMENTS

Magnetic field measurements on the Michigan State University cyclotron and analysis of the data obtained have been described in an MSUCP report[13], and will be summarized here to the extent necessary for understanding of subsequent material.

A thermoelectrically-cooled Hall probe with an accuracy of better than 5 parts in 100,000 was employed for the magnet measurements[14]. The Hall voltage was amplified, and digitized by a voltage-to-frequency converter and a frequency counter, and the resulting data punched automatically on cards; random error in the complete measuring system was kept below 1 part in 10,000. Using a deuteron NMR probe to monitor the field during all measurements, the magnet drift was observed to be less than 1 part in 10,000.

Measurements were made on a polar grid of points of one inch radial spacing at four degree azimuthal intervals[15]. The radial position was in most cases correct to within 0.001 inches, while the azimuthal position was controlled to about 0.005 degrees. The absolute azimuthal position was reproducible to within 0.005 degrees.

Variable-energy, multi-particle operation of a cyclotron imposes stringent demands on the accuracy with which the magnetic fields must be known over the entire excitation range of the magnet; magnetic field elements for the MSU machine consisted of the main magnet, eight pairs of concentric circular trimming coils, and a set of identical first harmonic coils located in each magnet "valley" near the position of the maximum average

or, alternatively, in terms of the Fourier amplitudes B_i:

$$B(r,\theta) = \langle B(r,\theta)\rangle + \sum_{n=1}^{3} B_{3n}(r)\cos 3n(\theta-\delta_{3n}(r)) + b_1\cos(\theta-\delta_1(r)), \tag{1-2}$$

where:

$$B_i(r) = \sqrt{H_i^2(r) + G_i^2(r)}, \tag{1-3}$$

and:

$$\delta_i(r) = \frac{1}{i}\,\mathrm{Arctan}\left|\frac{G_i(r)}{H_i(r)}\right| . \tag{1-4}$$

The seven sets of main magnet average field components $\langle B(r,\theta)\rangle$ were "smoothed" by a graphical procedure to within about 5 parts in 100,000; this procedure was chosen instead of a numerical device because it allowed discrimination against a known systematic error in the positioning device used in the measurements while rendering other data points unchanged. (See Reference 13 for details.) It was not necessary to apply any smoothing procedure to the flutter components since the effects on orbits due to the errors in the flutter smoothness are negligibly small. Studies showed that sufficient detail in the orbit properties could be obtained with a truncated Fourier representation consisting of only the average field, third, sixth, and ninth harmonics. Since the behavior of orbits in the vicinity of the $\nu_r = 1$ resonance depends very sensitively on the

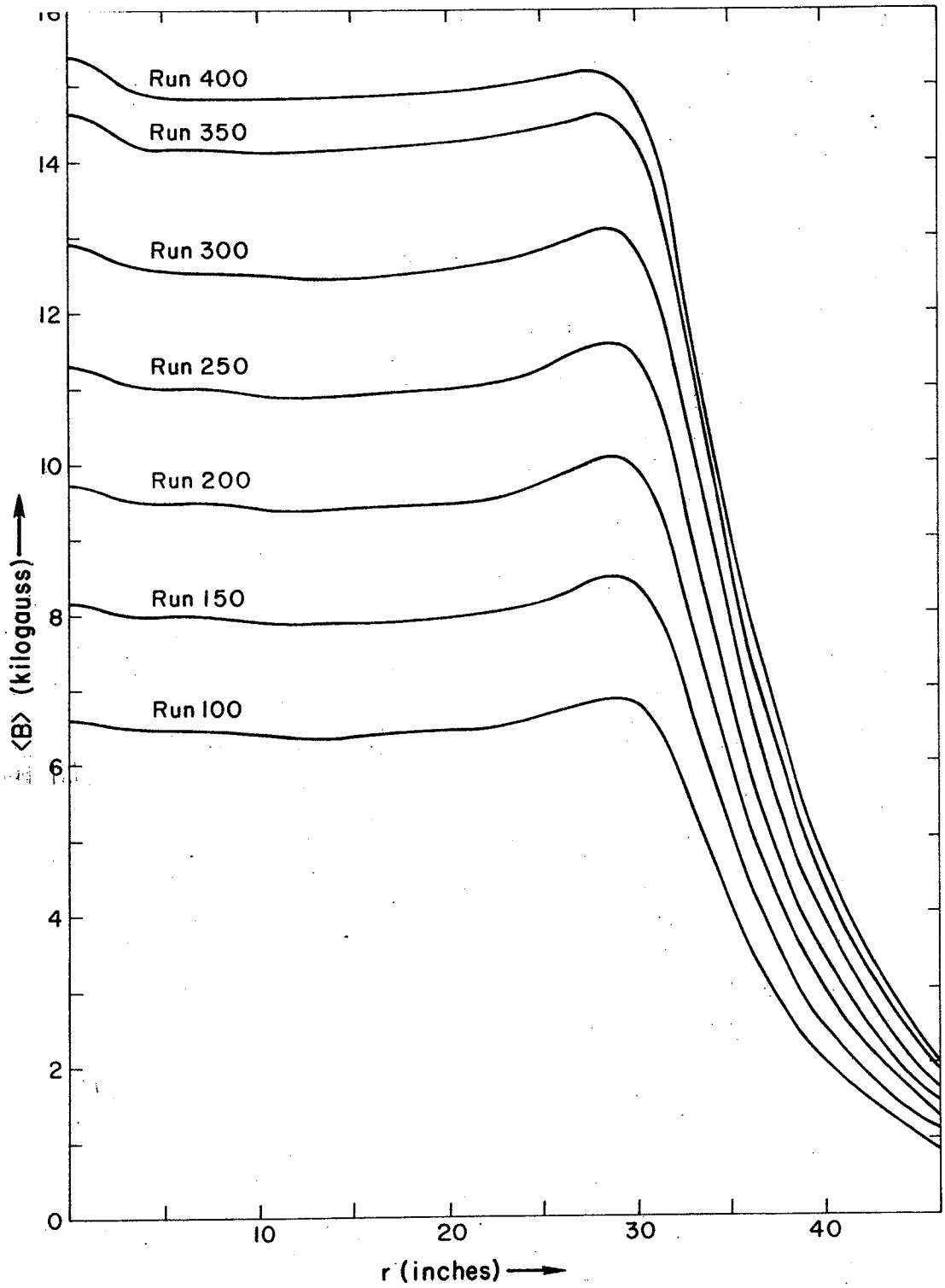

Figure 2. Azimuthal average of the magnetic field vs. radius for each measured excitation of the Michigan State University cyclotron.

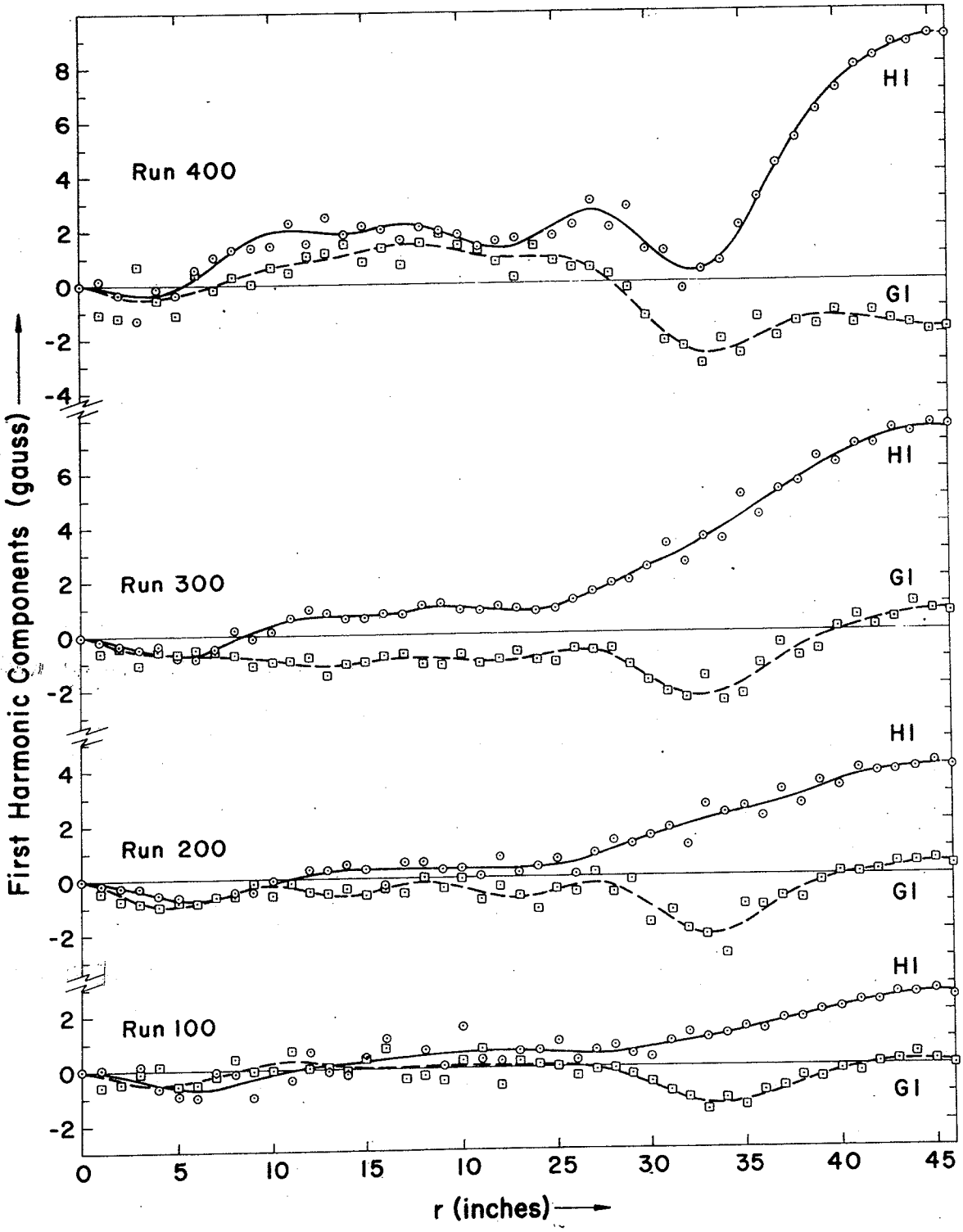

Figure 4. Magnetic field first harmonic sine and cosine Fourier components vs. radius for four main field excitations. Points show measured values; curves show result of smoothing computation. The large first harmonic at outer radii is due to main coil leads.

most cases, below 100 amps, as will be discussed later. Figures 5 and 6 show the incremental fields of the trim coils as a function of radius for each of the measured main field excitations.

In addition to the trimming coils which are concentric with the magnet pole, each valley of the magnet contains a small circular coil centered at a radius of 27 inches and used to control the first harmonic in the vicinity of the $\nu_r = 1$ resonance. The fields of these coils were found to closely approximate that of an air-core coil, with little change with main magnet excitation; thus it was deemed necessary to make field measurements for these valley coils at only two main magnet excitation values. A Fourier analysis of the incremental effect of the valley coil yielded the first harmonic sine and cosine components of its magnetic field. All other components were discarded; the coils are used with the algebraic sum of their currents equal to zero and thus produce no net average field component; other harmonics were found to be extremely small. Since the phase angle δ_1 of the first harmonic is relatively constant, a simplifying procedure was introduced in describing the valley coil first harmonic by a cosine component centered about the azimuthal position of the coil and thus possessing no spiral component, with a radial profile given by the measured cosine component. The data were smoothed graphically to within a few tenths of one gauss per 100 amps in the valley coil; the resulting radial profile of the valley coil first harmonic at both of the measured main field excitations is given in Fig. 7.

The resultant data were combined with ideal average fields,

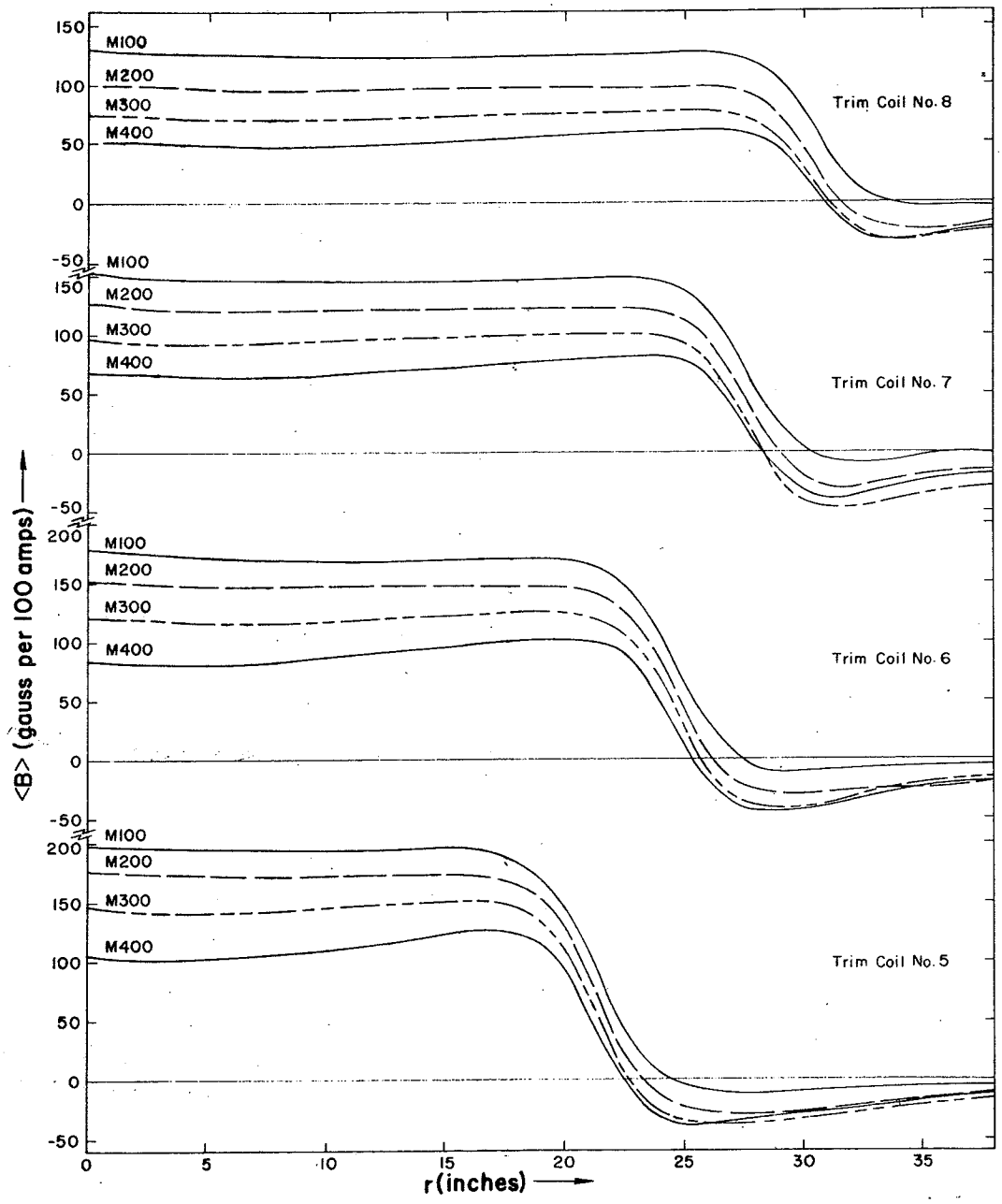

Figure 6. Average magnetic field vs. radius for trim coils 5-8 of the MSU cyclotron. Curves are shown for each trim coil for each of the four main field excitations at which the trim coil fields were measured.

obtained as described in the following section, to yield a "master" field deck, the data appearing as follows:

(1) Main magnetic field data at each of the seven measured main field excitations:

(a) Proton ideal average field.

(b) Deuteron ideal average field.

(c) $^{12}C^{4+}$ ideal average field.

(d) $^{3}He^{2+}$ ideal average field.

(e) "Heavy ion" ideal average field.

(f) Main magnet raw average field.

(g) Flutter field Fourier components H_3, G_3, H_6, G_6, H_9, G_9.

(h) First harmonic Fourier components h_1, g_1.

(2) Trim coil data: average field of each trim coil at each of the four main field excitations at which it was measured.

(3) Valley coil data: first harmonic components of one valley coil at each of the two main field excitations at which it was measured.

where δ is the angle of the peak hill field, and F is the flutter function, defined by:

$$F = \frac{\langle B^2 \rangle - \langle B \rangle^2}{\langle B \rangle^2} = \frac{1}{2} \sum_{i=3,6,9} \left(\frac{B_i}{\langle B \rangle} \right)^2 , \qquad (2\text{-}4)$$

where $\langle B \rangle$ is the average magnetic field Fourier component and the B_i are the magnetic field Fourier amplitudes defined by equation (1-3). The phase history of an accelerated particle may be related to the magnetic field (see Section 8 for more complete derivation) by the approximate equation:

$$\sin\phi(R) = \sin\phi(o) + \frac{2\pi q \omega_o}{E_1} \int_o^R [B_I(R) - \langle B(R) \rangle] R dR , \qquad (2\text{-}5)$$

where the phase ϕ is defined by:

$$\phi = \theta_{RF} - \theta_{Particle} , \qquad (2\text{-}6)$$

and q is the particle charge, ω_o is the RF angular frequency, E_1 is the maximum energy gain per turn and $B_I(R)$ is the isochronous average field.

Equations (2-1), (2-2), and (2-5) are given here only as approximate guides to aid in understanding the procedure used to obtain ideal fields. In practice, numerical integration of the complete equations of motion is used to obtain precise values of these functions, as is described later.

From equations (2-1), (2-2), and (2-5) one notes that the

face configuration (in the absence of flutter coils), the isochronous average field for a given ion is unique and can be calculated. Since the isochronous field automatically satisfies criterion (3) above, a first approximation to the desired ideal field was taken to be the isochronous average field, joined smoothly to the edge field at the radius of the peak average field. Given this first approximation field, the focusing frequencies were computed and inspected.

(2) For all fields, it was deemed desirable to increase the axial focusing at the center of the cyclotron more rapidly than could be obtained due to the rise in flutter alone. This problem had been anticipated in designing the pole tips, which were arranged to provide a focusing gradient in the average field in the central region. (See Fig. 2.) This natural focusing shape of the average field, conventionally referred to as a field "cone"[17], was effectively included in the ideal fields by the simple device of omitting the region of radius less than 5 inches from the fitting process. Such a cone results in a relatively large phase shift per turn, but this is acceptable because of the small number of turns in this region. Furthermore, the phase shift is useful in that it introduces desirable behavior into the phase history on the first few turns—to obtain large first order electric focusing on the early turns, it is customary[18] to start the particles at a phase of between 30° and 40°; the cone then shifts the phase to a value favorable for acceleration. (The cone also introduces a dip in the radial focusing frequency followed by a rise

tion which is typically less than two parts per 10,000 over the field region which is isochronized. Note that the main magnet has been designed to possess an average field whose increase with radius lies between the extremes needed for acceleration of the various particles thereby reducing overall trim coil loads. Also, note that the isochronous field in the central region decreases with radius due to higher order effects involving the flutter gradient; this drop extends over half radius in the case of the heavy ions.

2.2 Axial Focusing Correction

For the high-energy proton fields it was necessary, as indicated previously, to de-isochronize the field to obtain axial focusing. The following equations are given as a guide to aid in understanding the method used. Approximations are used to initially obtain the average field correction; the validity of the approximations is then checked by exact computations using the equilibrium orbit code.

From before:

$$\nu_z^2 = - k(R) + F(R)[1+2\tan^2\alpha(R)], \qquad (2\text{-}2)$$

where:

$$k(R) = \frac{R}{\langle B\rangle}\frac{d\langle B\rangle}{dR} . \qquad (2\text{-}9)$$

field, equation (2-2) may be written as:

$$\nu_z^2 = - k(R) + \frac{\Delta(R)}{\langle B \rangle^2} \quad , \tag{2-11}$$

where $\Delta(r)$ is independent of average field. Defining $u = \langle B \rangle^2$, and using primed variables to indicate the desired values for ν_z and the average field gives:

$$\frac{d}{dR}(u'-u) = - \frac{2}{R}\left[\nu_z'^2(u'-u) + u(\nu_z'^2-\nu_z^2)\right] . \tag{2-12}$$

This can be rewritten as:

$$\frac{dy}{dR} = p(R)y + q(R) \tag{2-13}$$

where $p(R)$ and $q(R)$ are known functions of the old and new axial focusing frequencies. Solution of the differential equation for $y = u'-u = \langle B' \rangle^2 - \langle B \rangle^2$ gives the correction to the average field necessary to produce the desired ν_z. A corrected field was calculated over the range of radii where the axial focusing was insufficient. Smooth connection of the corrected average field to the isochronous average field was accomplished at the outer radius by means of the starting conditions chosen for the integration. The average field below the corrected region was joined smoothly to the corrected region by scaling the isochronous field for all radii inside the corrected region.

An example of such a calculation is shown in Fig. 10 for

the case of 52 MeV protons: part (a) shows the isochronous average field and the new average field resulting from correction of the axial focusing frequency of the isochronous field; part (b) shows the axial focusing frequency of the isochronous field and that of the corrected field; part (c) shows the sine of the phase slip of an accelerating particle versus radius for a starting phase of + 30° for both the isochronous field and the corrected field. The RF frequency in each case has been adjusted to minimize the energy spread in the beam at the extraction energy of 52 MeV. Both the axial focusing frequencies and the phase history data were obtained from the equilibrium orbit code.

The results indicate that this relatively simple procedure is quite adequate as an alternative to the use of flutter coils. The resulting field is satisfactory as regards all of the criteria stated in Section 2; in addition, the energy spread at extraction is kept within desired design limits and the phase of the particles with respect to the RF voltage at the extraction energy is kept small enough to retain ideal extraction properties.

2.3 Radial Focusing Correction

It is convenient in determining extraction parameters for the radial oscillation frequency to be a "similar function" of radius in the edge region for the entire range of

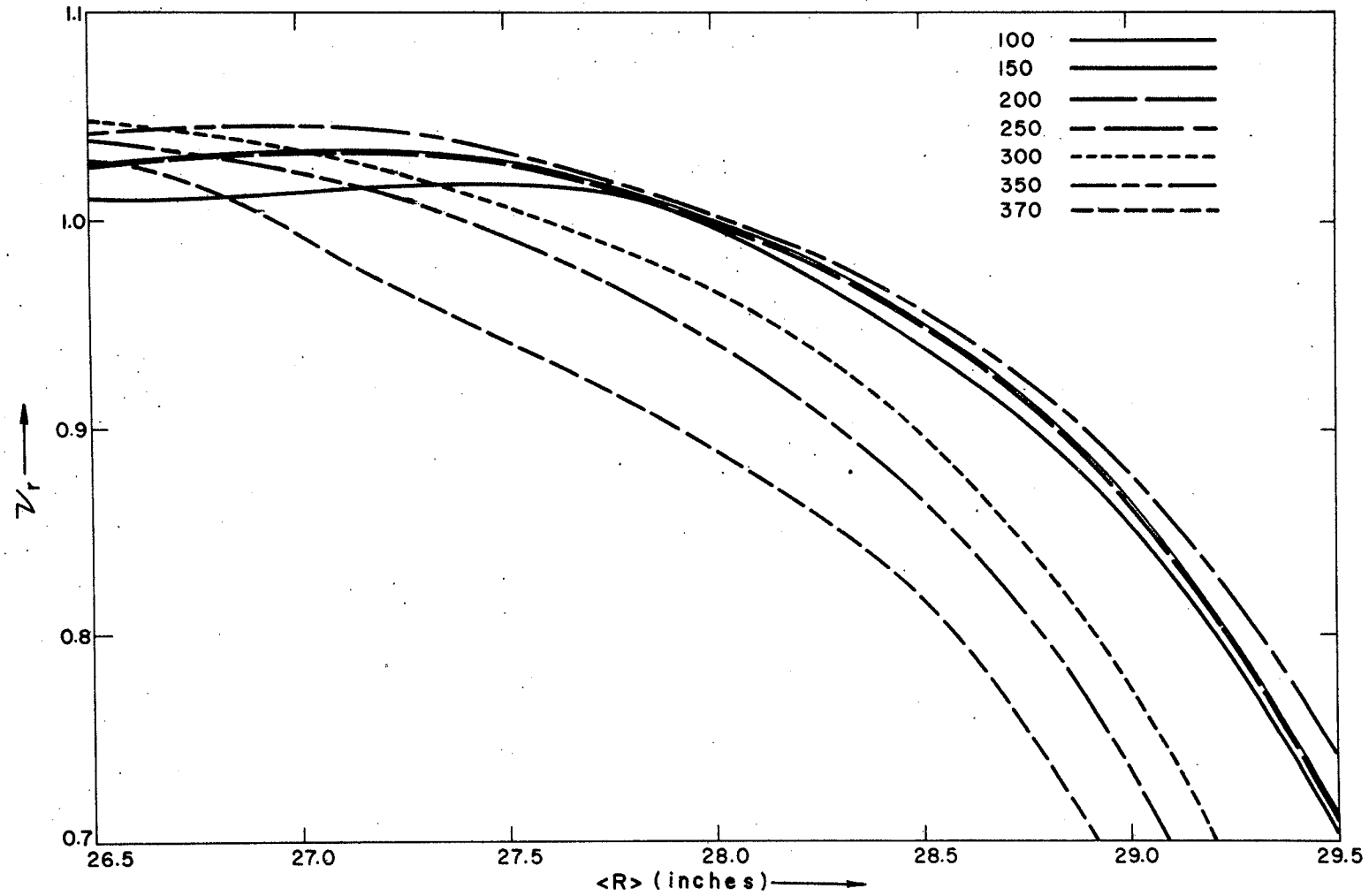

Figure 11. ν_r vs. radius for the set of proton isochronous average fields (corrected to provide axial focusing for energies above 42 MeV) at the measured main field excitation values.

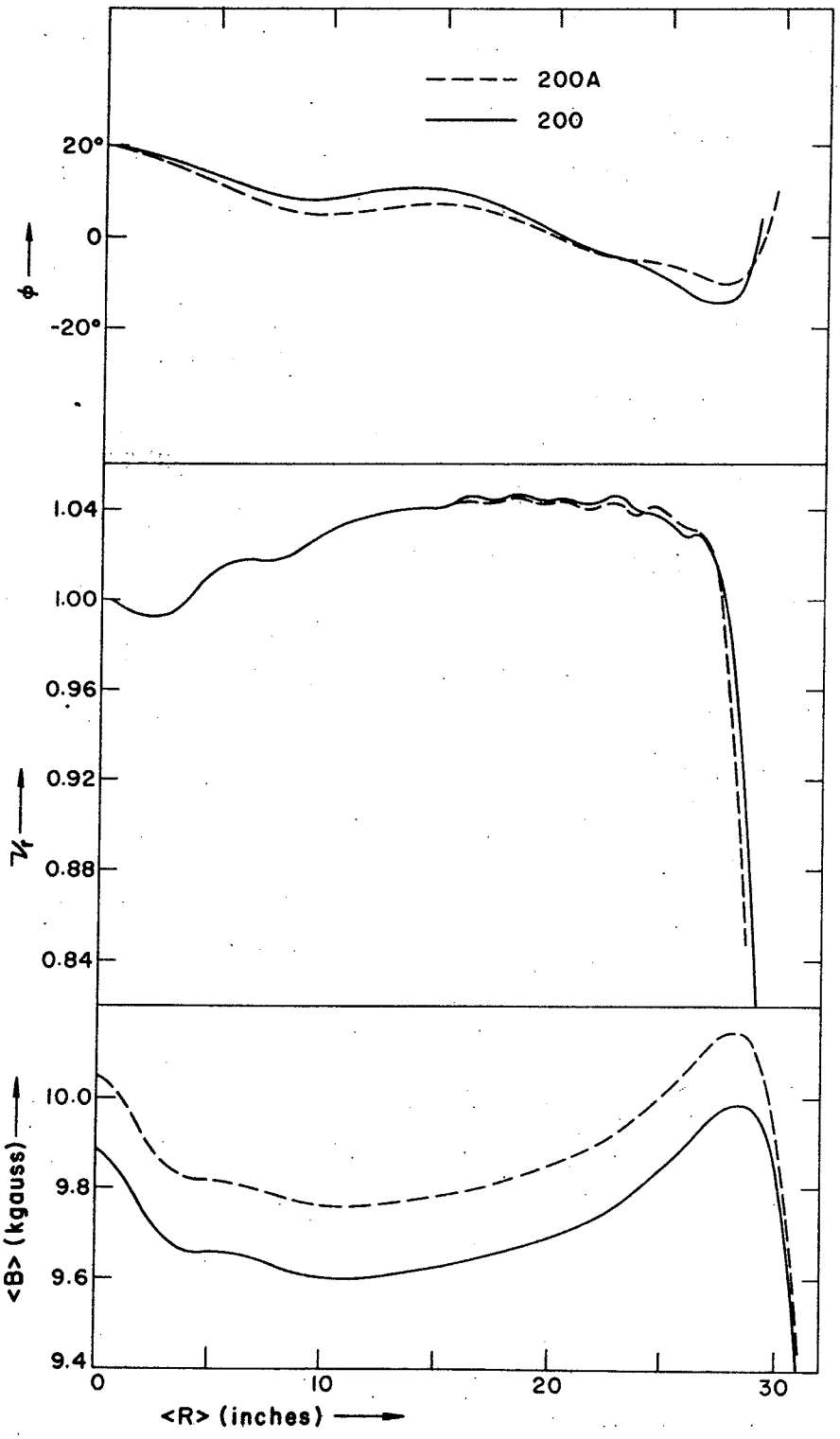

Figure 12. <B>, ν_r, and ϕ for fitted fields before (200) and after (200A) correction of ideal average field to provide uniformity of ν_r in the edge region.

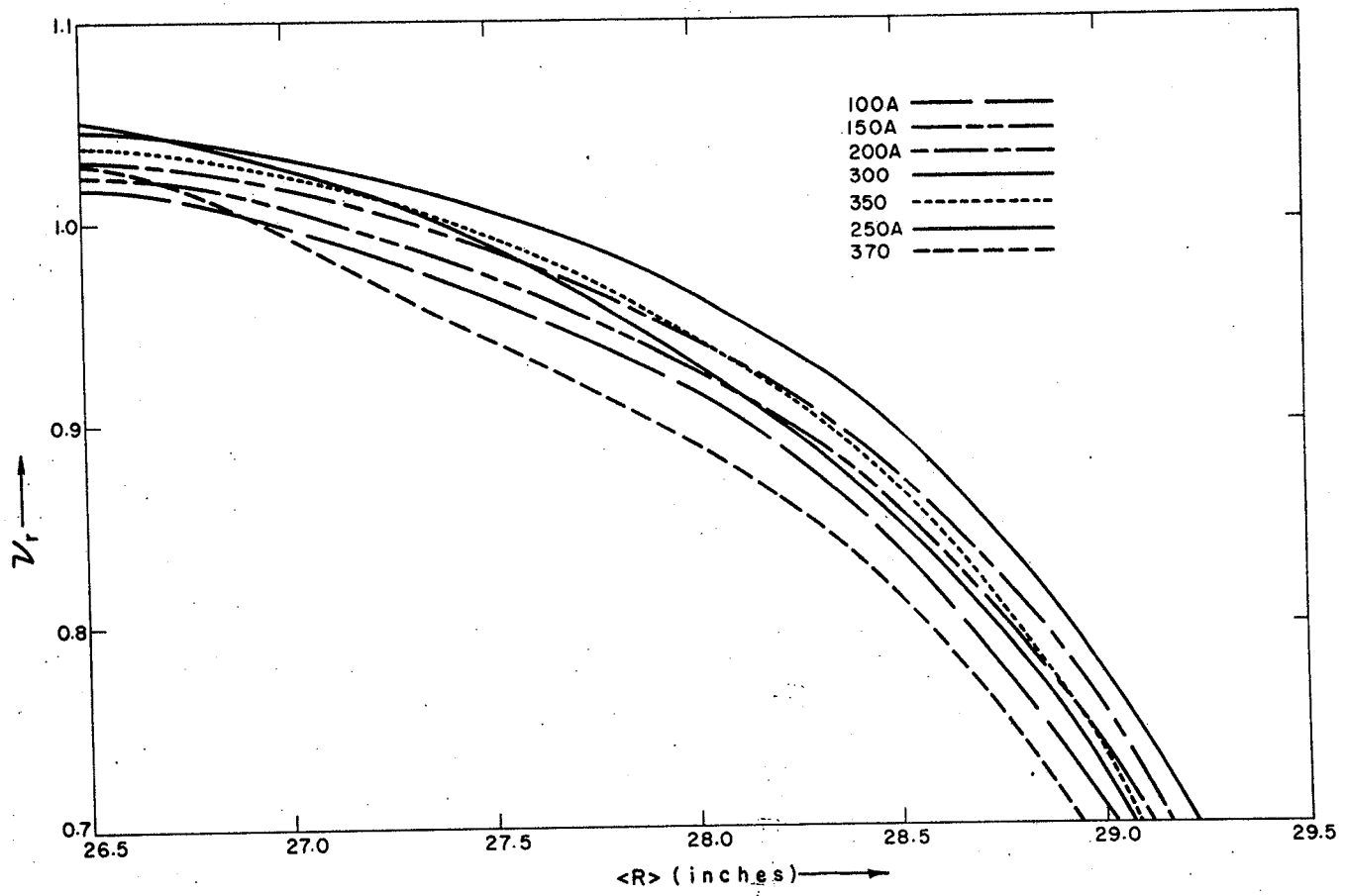

Figure 13. ν_r vs. radius for the ideal proton fields shown in Figure 11 after correction of the ideal average fields for main magnet excitations 100, 150, 200, and 250 (less than 33 MeV protons) to render ν_r in the edge region a similar function to that of field 350 (52 MeV protons).

(5) The resulting scheme should be as simple as possible; it should be fast and well-adapted for use on a computer due to the large number of interpolations which must be performed for each set of fields.

It also seems desirable that as little of the data as possible should be used in defining a particular intermediate result—due to the complex dependence of the saturation of the iron as a function of excitation, it seems reasonable to suppose that use of the data for low excitations, for example, would be of little aid in determining fields at the high excitation values.

Among the procedures considered were various order Lagrangian polynomial interpolations, various types of spline interpolation[22], and interpolation using polynomials obtained from fitting the data, which redefines the measured points as well as intermediate values by passing the best least squares curve through the data. Unfortunately, strict Lagrangian polynomial interpolation results in appearance of the ubiquitous polynomial wiggles, especially when high-order interpolation is used. For example, use of four-point Lagrangian interpolation to obtain trim coil average fields often results in distinct wiggles characteristic of a cubic polynomial, thereby introducing both unphysical field data at intermediate excitation values as well as discontinuities in the field derivatives at the measured field points. Therefore, it is desirable to reduce the number of points used in such a procedure as much as possible.

where $f_{lower}(x)$ and $f_{upper}(x)$ are given by three-point Lagrangian interpolation:

$$f_{lower}(x) = \sum_{i=1,2,3} \prod_{\substack{j=1,2,3 \\ j\neq i}} \left(\frac{x-x_j}{x_i-x_j}\right) f(x_i) \ , \qquad (3\text{-}2)$$

$$f_{upper}(x) = \sum_{i=2,3,4} \prod_{\substack{j=2,3,4 \\ j\neq i}} \left(\frac{x-x_j}{x_i-x_j}\right) f(x_i) \ . \qquad (3\text{-}3)$$

One limitation on this procedure is that it cannot be used in the extreme intervals of the measured data points. Therefore, straight three-point Lagrangian interpolation has been used in these regions in order to join the data smoothly while introducing a minimum of interpolation error. In practice no noticeable discontinuity resulted, nor were interpolation problems observed. Several of the Lagrangian polynomial methods were checked by computing difference tables for field functions obtained by interpolation using each method; the double three-point continuous derivative formula was found to yield the smoothest function over the entire range in that it gave the smoothest difference functions.

Choice of the particle extraction energy as the independent variable for interpolation was dictated by practicality and simplicity in labeling resulting fields. In each of the measured fields, an operating point was computed, where for each field the extraction energy was determined on the basis of orbit properties in the extraction region, which will be discussed later. (See Section 6.) Assigning this extraction

fective field at that excitation is synthesized by summing the Fourier data.

Other results of the interpolation method used as they apply to over-all operating point computations are discussed in Section 7.

taneously adjusting trim coil currents, main field excitation, and RF frequency and voltage, subject to arbitrary constraints on the phase excursion, final energy, ν_r and ν_z. The method uses approximate equations to compute the phase and the betatron frequencies, so that no previous calculation is necessary to obtain ideal fields. In the limit, this extremely powerful method can be used to adjust any cyclotron parameter which can be expressed in an appropriate mathematical form.

Because of the versatility of the linear programming method, it is necessarily complex; therefore, if a problem in orbit properties arises, it is quite difficult to isolate the cause of such a problem and work on this problem independently. Furthermore, while results for the various parameters for any given operating point yield acceptable orbit properties for the given field, when taken in total, discontinuities in the various operating points occur over small excitation intervals.

A total operating point calculation using least squares fitting to obtain trim coil currents was chosen for several reasons. Although it is necessary to carefully pre-determine ideal fields, the fits obtained using least squares are extremely accurate, and field errors giving rise to differences between orbit properties in ideal and fitted fields are generally kept below the accuracy with which the magnetic fields are known. Therefore, since ideal fields possessing good beam properties are specified, fitted fields, as well, possess these desirable properties. Adjustment of RF frequency can be

set of trim coil currents.

Given the average fields per unit ampere of the N trim coils at L radii $b_n(r_\ell)$, the ideal difference average field $E(r_\ell)$, and an arbitrary weight factor $\rho(r_\ell)$, the quantity δ can be formed, where:

$$\delta = \sum_{\ell=1}^{L} \rho(r_\ell) \sum_{n=1}^{N} [a_n b_n(r_\ell) - E(r_\ell)]^2, \qquad (4\text{-}1)$$

where the a_n are the desired trim coil currents. The least squares criterion may then be stated as calculation of the a_n such that δ is minimized, or as a set of N simultaneous linear equations:

$$\frac{\partial \delta}{\partial a_i} = \sum_{\ell=1}^{L} \rho(r_\ell) b_i(r_\ell) \sum_{n=1}^{N} [a_n b_n(r_\ell) - E(r_\ell)] = 0 \ , \qquad (4\text{-}2)$$

for i = 1. . .N. This can be reduced to the matrix equation:

$$\underline{X}\ \underline{A} = \underline{B} \ , \qquad (4\text{-}3)$$

where $\underline{X}$ is the N x N dimensional matrix:

$$\underline{X}_{in} = \sum_{\ell=1}^{L} \rho(r_\ell) b_i(r_\ell) b_n(r_\ell) \ , \qquad (4\text{-}4)$$

$\underline{B}$ is the N-dimensional column vector:

$$\underline{B}_i = \sum_{\ell=1}^{L} \rho(r_\ell) b_i(r_\ell) E(r_\ell) \ , \qquad (4\text{-}5)$$

and $\underline{A}$ is the N-dimensional column vector of the desired trim

viously, the central region (0-5 inches) is omitted in order to preserve the field "cone" of the untrimmed fields and thereby increase ν_z in the first turns. The maximum radius was set at 28 inches which is both the maximum radius of useful orbits and also the radius beyond which the difference field between the ideal average field and the main magnet average field is essentially zero. Through this choice of radii, the field fitting was concentrated in the region where most of the acceleration occurs, while allowing the contribution of the trim coils to fall off naturally in the edge region, where the coils inherently have little effect. (See Figs. 5 and 6.)

Provision was also included for introduction of weighting factors which could be used to provide greater fitting accuracy in any desired radius region. However, in a test of this device, a weighting factor which weighted each radius by the turn density in that region was introduced with essentially negligible effect. This can be attributed to the fact that the fit is in any case exceedingly good, and a relatively large weighting factor is required to significantly effect the fit in any region.

A pleasant feature of the fitting in actual practice was a lack of large approximately equal currents of opposite sign in neighboring coils, which often are obtained in least squares fitting; this is partially a result of the fact that the fields that the trim coils are fitting are smooth, monotonic functions of radius with no sign changes.

Examples of results of this field fitting procedure are

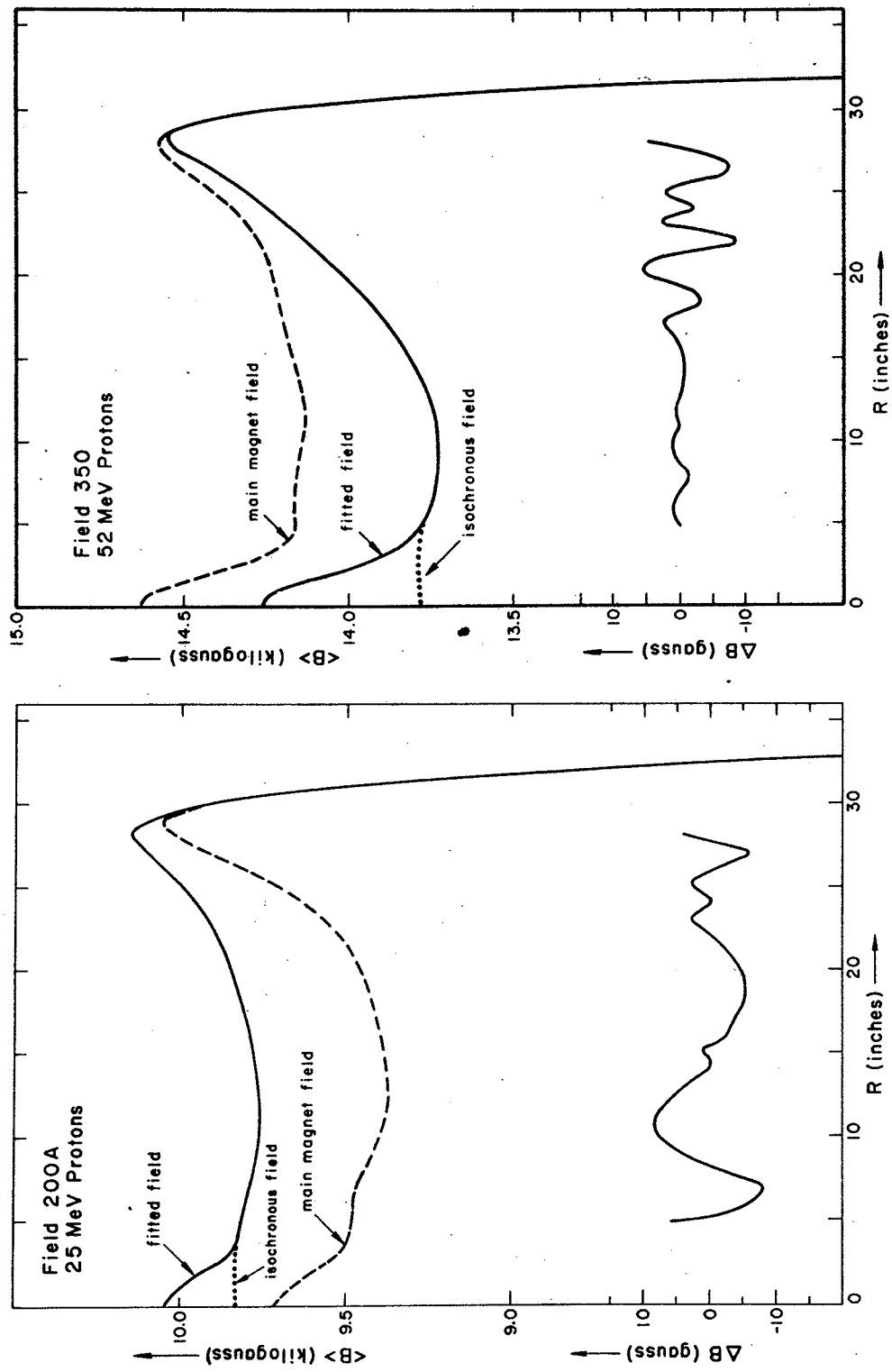

Figure 14. Average fields obtained by the modified least squares procedure for 25 and 52 MeV protons. Ideal average fields, main magnet average fields and fitted average fields are shown, along with the resulting error fields in the interval over which the fit was performed.

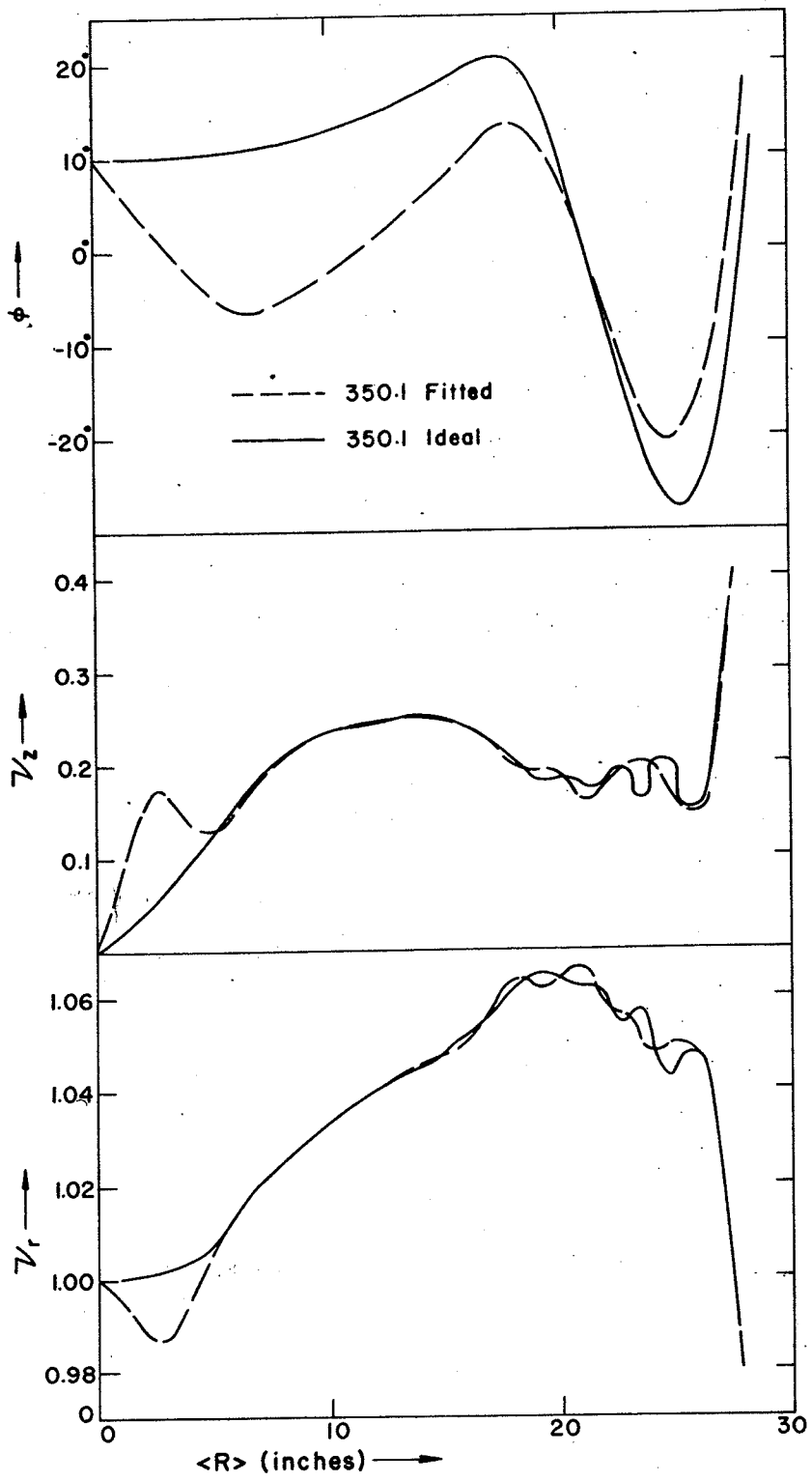

Figure 16. Comparison of ν_r, ν_z, and ϕ vs. radius with ideal average fields and fitted average fields for 52 MeV protons.

Defining the phase of the particle ϕ with respect to the RF accelerating voltage:

$$d\phi = \omega_o dt - h d\theta \tag{5-1}$$

where ω_o is the RF angular frequency, h is the harmonic number, t is absolute time and θ is particle angle, the phase change per turn is given by:

$$\frac{d\phi}{dN} = 2\pi\left(\frac{\omega_o}{\omega} - h\right) , \tag{5-2}$$

where N is the turn number. The energy gain per turn is related to the phase through the equation:

$$\frac{dE}{dN} = E_1 \cos\phi(E) \tag{5-3}$$

where E_1 is the maximum energy gain per turn, which is a function of dee voltage and RF mode. Combining equations (5-2) and (5-3), one obtains the longitudinal differential equation of motion relating E and $\phi(E)$:

$$\frac{dE}{d\phi} = \frac{dE/dN}{d\phi/dN} = \frac{E_1 \cos\phi(E)}{2\pi\left(\frac{\omega_o}{\omega} - h\right)} . \tag{5-4}$$

Integrating this differential equation yields:

$$\sin\phi(E) = \sin\phi_o + \frac{2\pi h}{E_1} \int_0^E \left(\frac{\omega_o}{h\omega} - 1\right) dE , \tag{5-5}$$

i.e., by requiring:

$$\int_{0}^{E} \sin\phi(E)dE = 0 \qquad (5\text{-}10)$$

However, as will be seen from data presented later, in order to obtain strictest control over the energy spread, it is necessary to carefully adjust the frequency beyond this first approximation obtained by balancing the phase integral.

For an arbitrary field, for a band of phases symmetrical about a starting phase ϕ_o the energy vs. phase for a sequence of turn numbers defines a series of so-called "energy parabolas", and the problem of minimizing energy spread is reduced to the problem of computing a fractional frequency correction ε such that the central ray lies at the position of the peak of the energy parabola for a given final energy. Mathematically, an ε must be found such that:

$$\left(\frac{\partial E}{\partial \phi_o}\right)_{\varepsilon,N} = 0 \qquad (5\text{-}11)$$

This is equivalent to maximizing the energy for a given number of turns, or to minimizing the number of turns in the central ray to obtain a given final energy. In particular, for single turn extraction, the energy spread should be much less than the energy gain per turn in the extraction region. Following the rules for partial derivatives, after considerable manipulation the following relation may be derived:

thus lies on a cosine curve, where the position of the energy peak of the curve is a function of turn number; after N turns the central ray attains the position of peak energy, with symmetrical distribution of the energy about the central ray, and the energy spread for a phase distribution of $\pm \delta\phi$ about starting phase ϕ_o is a minimum.

Figure 17 shows the results obtained from the computer program "PHINAL" for the energy of a beam of particles of 6^o phase width centered about a central ray of $\phi_o = 30^o$ as a function of turn number for the 25 MeV and 52 MeV fields previously discussed. The frequency has been adjusted to yield minimum energy spread at the indicated energies; the energy parabolas can be clearly observed to peak at the appropriate energy. The result of the energy spread minimization is most striking for 52 MeV protons, since the field deviates considerably from isochronism; the 25 MeV field is essentially isochronous to the edge region. With a band of starting phases of 6^o width, which is readily attainable on the MSU machine using the central slit mechanism, energy spread in the extracted beam may be reduced to the design value of 0.1%. It should be noted that minimization of the energy spread at a given final energy does not preclude the possibility of an absolute minimum in the energy spread at a later turn number; however, the geometry of the extraction region as well as the diminishing energy separation between successive turns necessitates extraction at the earlier energy.

Another important feature of the "PHINAL" code is the calculation of a set of frequency limits which drive the central ray of the beam out of phase with the RF accelerating voltage at various energies. From equation (5-9), it is clear that if the frequency is varied such that the phase is allowed to go to $\pm 90^{\circ}$, then $\sin\phi(E) = \pm 1$, and since E_1, $\sin\phi$ and $F(E)$ are known, for a given final energy E, the frequency correction ε, and thus the frequency, is uniquely defined. Validity of these results and their use are discussed in later sections.

discussed sequentially below—basic theoretical considerations have been discussed previously.

1. Magnetic Field Interpolation

All magnetic field data are stored as tables of Fourier coefficients at each measured main field excitation. The Fourier components at the desired intermediate excitation are computed by interpolation in the measured field data using the specified energy as the independent variable for the interpolation, where an energy value has previously been assigned to each measured field on the basis of orbit computations in the fitted fields. A complete set of Fourier coefficients for the resulting field is provided for possible use in independent orbit studies as well as to check the accuracy of the field computations and data handling. The set of cyclotron units are defined by taking the ideal field at machine center as the field unit.

2. Average Field Fitting

A modified least squares fit of the trim coil average fields to the difference field between the ideal average field and the main magnet average field is performed to determine trim coil currents for the eight sets of concentric circular trim coils; the fit covers the region from 5 inches

The RF harmonic number is taken to be the lowest possible within the frequency limits of the RF system using the cyclotron unit of frequency as a first approximation; the dee voltage is then computed:

$$h = 1: \; V_D = \frac{E_1}{4\cos 21^\circ}$$

$$h = 2: \; V_D = \frac{E_1}{4\sin 42^\circ}$$

$$h = 3: \; V_D = \frac{E_1}{4\cos 63^\circ}$$

4. Adjustment of RF Frequency

Using the equilibrium orbit orbital frequency data, and a given starting phase, a correction to the RF frequency is computed which minimizes the energy spread in the beam for a single turn at the extraction energy. A table of minimum and maximum frequencies as a function of energy for reducing the beam to half amplitude when the RF voltage is held constant is also provided as an aid in beam diagnosis using RF variation. (This is equivalent to driving the central ray out of phase with the RF as discussed in Section 5.)

7. Trim Coil Current Limits

A set of trim coil currents which drive the beam to half amplitude at various specified radii are computed; these data are useful in setting up the cyclotron main field and can be compared to experimental data taken in phase measurements.

8. SETOP Sheet

A final output sheet contains cyclotron control settings arranged in a manner convenient for use by an operator in setting up the cyclotron.

VII. RESULTS OF OPERATING POINT COMPUTATIONS

The information given by the SETOP program consists of two segments: (1) a series of results of intermediate calculations useful in cyclotron orbit studies and in diagnosis of any eminent problems, and (2) a summary sheet which enables the individual experimenter to successfully operate the machine by tabulating the various operational parameters in terms of simple dial settings. The results of intermediate calculations have been given previously in discussion of the various sections of the program.

A sample of the cyclotron operating point summary sheet is shown in Fig. 18. Each sheet is labeled by the particle and energy of interest. The main field is given in terms of the main magnet current and the voltage obtained by a rotating coil fluxmeter used to monitor the magnetic field. RF data includes frequency, harmonic and mode, and the dee voltage; the number of turns is given as an aid in obtaining the correct dee voltage. Trim coil "cut-off" currents at 24 inches are given as a method of setting the main field more accurately than is possible with the fluxmeter. Trim coil and valley coil data are given in terms of dial readings on their respective panels. First harmonic data are given in terms of the cyclotron control settings, bump amplitude and azimuth, in two parts. The first harmonic necessary to cancel the intrinsic first harmonic at the $\nu_r = 1$ resonance is used in setting up the operating point. For extraction the

vector sum of the cancellation first harmonic and the desired extraction first harmonic is used, thus producing the stated desired value as the net first harmonic.

When the cyclotron has been properly adjusted, turn structure is clearly visible out to the extraction region, which indicates the accuracy of the calculations, stability of the RF voltage, and the small beam phase width obtained by the use of central region slits. In each case the computed values of the operating parameters have allowed acceleration of the beam to full radius without additional adjustment, and in no case has deviation of any of the operating parameters from their computed values resulted in better beam properties[26].

Of particular interest in a variable energy cyclotron is attainment of a uniform beam over a continuum of energy range, or by small energy increments over the range. It has been found that use of the procedure described results in a series of operating points where the parameters vary smoothly with energy. As an example, Fig. 19 shows the currents in the eight trimming coils as a function of field number for proton fields over the entire range of excitation. From this data it can be seen that it is possible to obtain essentially a continuum of proton fields while performing only a limited number of complete operating point calculations. It is clear from the data given in Fig. 19 that the smoothness of the trim coil currents will give continuous energy variation by interpolation in a relatively small num-

ber of fully calculated points; an appropriate system is now being installed in the MSU cyclotron laboratory computer[27]. Other parameters such as the RF frequency and dee voltage and the main magnetic field are found to vary equally smoothly and are similarly adaptable for interpolation. Small discontinuities enter because of the minimum current limit requirements, but such discontinuities are small and can be dealt with in a relatively straightforward manner.

Through adequate prior calculations of ideal fields (and ultimately through model magnet studies), acceptable beam properties have been obtained over the entire excitation range. The smooth variation of both the extraction energy and the position of the $\nu_r = 1$ resonance with field excitation indicates the uniformity which the field shape retains. The small phase gain or lag per turn indicates the accuracy of the field fitting procedure, and is further evidence that the quality of the interpolated ideal average field data is essentially as good as that of the computed data at the measured excitations. In summary, Figs. 20, 21, and 22 show, respectively, radial focusing frequency ν_r, axial focusing frequency ν_z, and phase history as a function of radius for a rather complete family of proton operating points including both measured and interpolated fields.

Results of beam measurements are in excellent agreement with pre-computed data, and confirm the quality of the calculations, as is discussed in the following section.

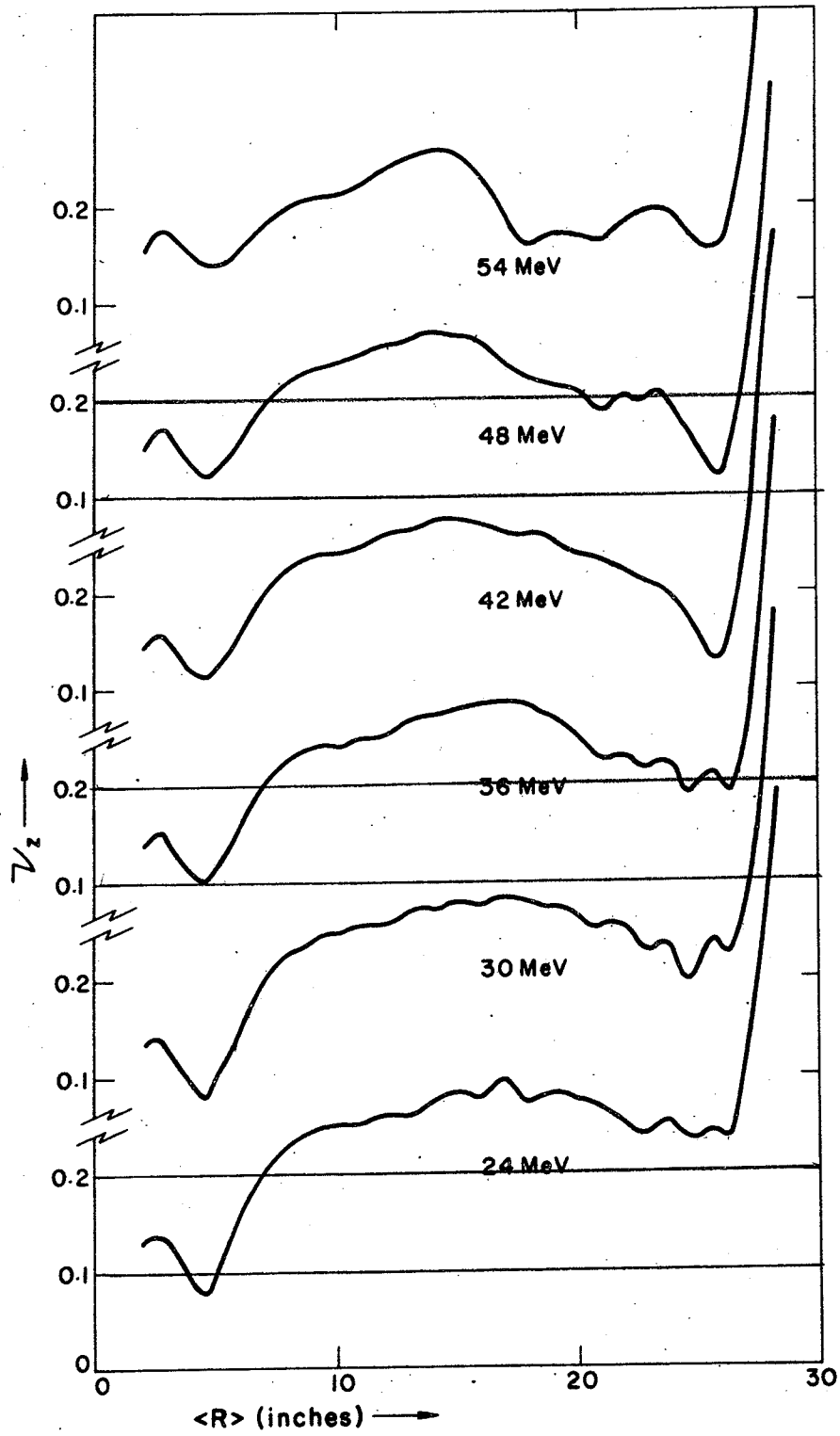

Figure 21. ν_z vs. radius for computed proton fitted fields covering the energy range accessible using rf first harmonic acceleration.

VIII. ORBIT STUDIES

Properties of orbits in MSU cyclotron fields have been investigated using a very precise orbit integration program known as CYCLONE[28]; orbit properties obtained from CYCLONE are compared with results from the approximate methods used in SETOP. CYCLONE utilizes exact median plane equations of motion to track accelerated orbits in the magnetic field specified by SETOP. Details of the electric field are accounted for in three ways, depending on the level of significance of the electric field: (1) source-to-puller region, in which the electric field is obtained from a large-scale model electrolytic tank including exclusively the source-to-puller region; (2) "RF focusing" region, in which the finite width of the accelerating gaps is obtained by using a more complete electrolytic tank to obtain the electric fields covering approximately the first four turns; (3) the outer region, in which the electric field is approximated by a time-dependent step-function potential. CYCLONE also includes provisions for both an electrostatic deflector and a magnetic channel, and thus is capable of demonstrating behavior of orbits in the cyclotron from ion source through the complete extraction system.

Using CYCLONE in combination with various other orbit programs, a theoretical investigation has been made of several of the procedures used regularly for beam diagnostic work. Particular attention has been devoted to problems

during a precession cycle. These errors will be shown to be exceedingly small for conditions of normal operation of the MSU cyclotron. Discrepancies between the approximate theory and exact orbit integration arise primarily from coupling effects which are essentially incalculable except through such orbit integrations; these discrepancies lead to limitations in the application of the methods discussed only in certain circumstances.

Possible errors in actual practice arise from: (1) encounter of resonances or, in the case of trim coil adjustment, introduction of additional resonances, which results in large centering errors, and violates the assumptions necessary to separate the longitudinal equation of motion by introducing coupling terms and non-uniqueness of the radius-energy function, and (2) in the case of trim coil variations, further deviation is introduced into the radius-energy function due to average field variation.

The problems outlined here are of special concern to the operating point calculations described for two primary reasons: (1) the operating point set-up procedure makes use of the device of trim coil detuning to set the main field, and (2) in order to set the main field precisely and determine the RF frequency precisely, it is necessary to know the starting phase with substantial precision.

An example indicating the accuracy of the longitudinal equations under ideal circumstances is given in Table 1 for a 42 MeV proton field; energy and phase are tabulated as a

function of turn number (at 10 turn intervals) for actual integrated orbits obtained from CYCLONE, and compared to the energy and phase obtained from SETOP by integrating the separated longitudinal equations (from Section 5):

$$\sin\phi(E) = \sin\phi_o + \frac{2\pi}{E_1}\int_o^E \left(\frac{\omega_o}{\omega} - 1\right) dE = \sin\phi_o + \frac{F(E)}{E_1} \quad , \quad (8\text{-}1)$$

and:

$$\frac{dE}{dN} = E_1 \cos\phi \quad , \quad (8\text{-}1a)$$

where the $\frac{\omega_o}{\omega} - 1$ values are obtained from the equilibrium orbit code. The integrated orbit in this case possessed a radial oscillation amplitude of approximately one millimeter; this behavior can be obtained on the MSU cyclotron by proper adjustment of central region parameters. Also given is the quantity $\Delta F(E)$ which is the difference between the F(E) values obtained from the two methods of integration. The small amplitude of $\Delta F(E)$ indicates the quality of the agreement; the fact that $\Delta F(E)$ oscillates with a period corresponding to the radial precession cycle indicates that the small errors present result from centering effects, particularly in the central region and at large radii. Errors as small as those in the table are of negligible effect in setting up the cyclotron. This result and the results of other examples verify the validity of the longitudinal equation under ideal

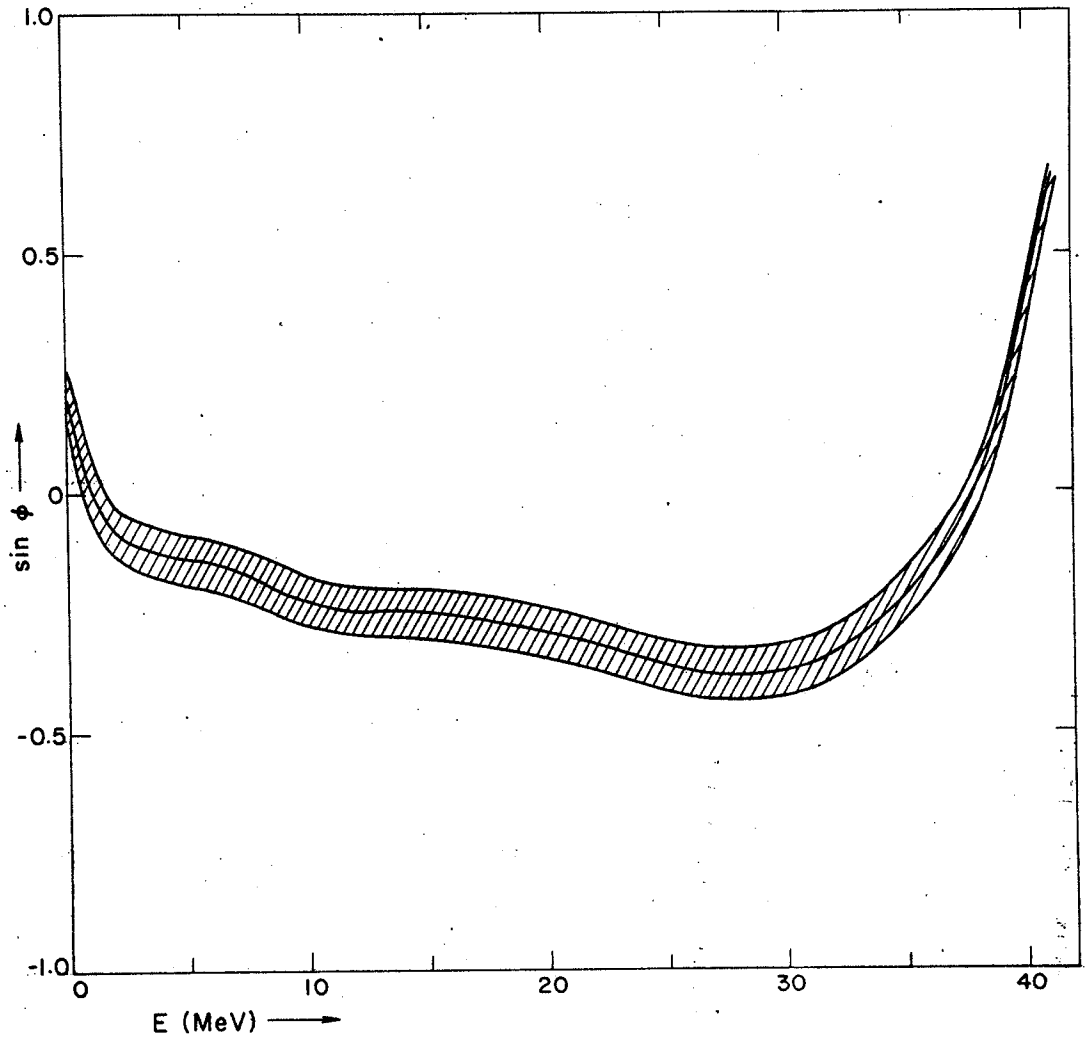

Figure 23. Sinϕ vs. E for a phase group of 6° width in Field 300 (42 MeV protons).

of the radial oscillation amplitude to below one millimeter raises the phase at which the orbit reaches its maximum radius to above 85°. One assumption used in obtaining equation (8-5) is that the radius is a function of energy alone, and not of turn number or frequency; this assumption is checked in calculations summarized by Table 2, for the same 42 MeV proton field, from results of a family of CYCLONE orbits. The effect of the small radial oscillation can be seen directly in the variation of radius at a particular energy, and the necessity of minimizing this effect becomes apparent. The conditions shown here are essentially identical to those obtained in the operation of the cyclotron. It should be noted that the oscillation is introduced through the starting conditions, and is not amplified by detuning of the system. It should also be noted that due to the gap crossing resonance[30], it is not possible to center the beam at all radii simultaneously; therefore, starting conditions should be used which center the beam at large radii, where the turn density is greatest.

Another limitation in applying the frequency detuning method at large radii arises from the particular shape of the $\sin\phi$ versus radius curve and its effect on the minimum frequency ω_- as a function of radius. Figure 24 shows the envelope of maximum and minimum frequencies as a function of radius for a 33.5 MeV proton field. Because the phase curve rises rapidly at large radii, the frequency required to drive the phase of the central ray to -90° is a constant

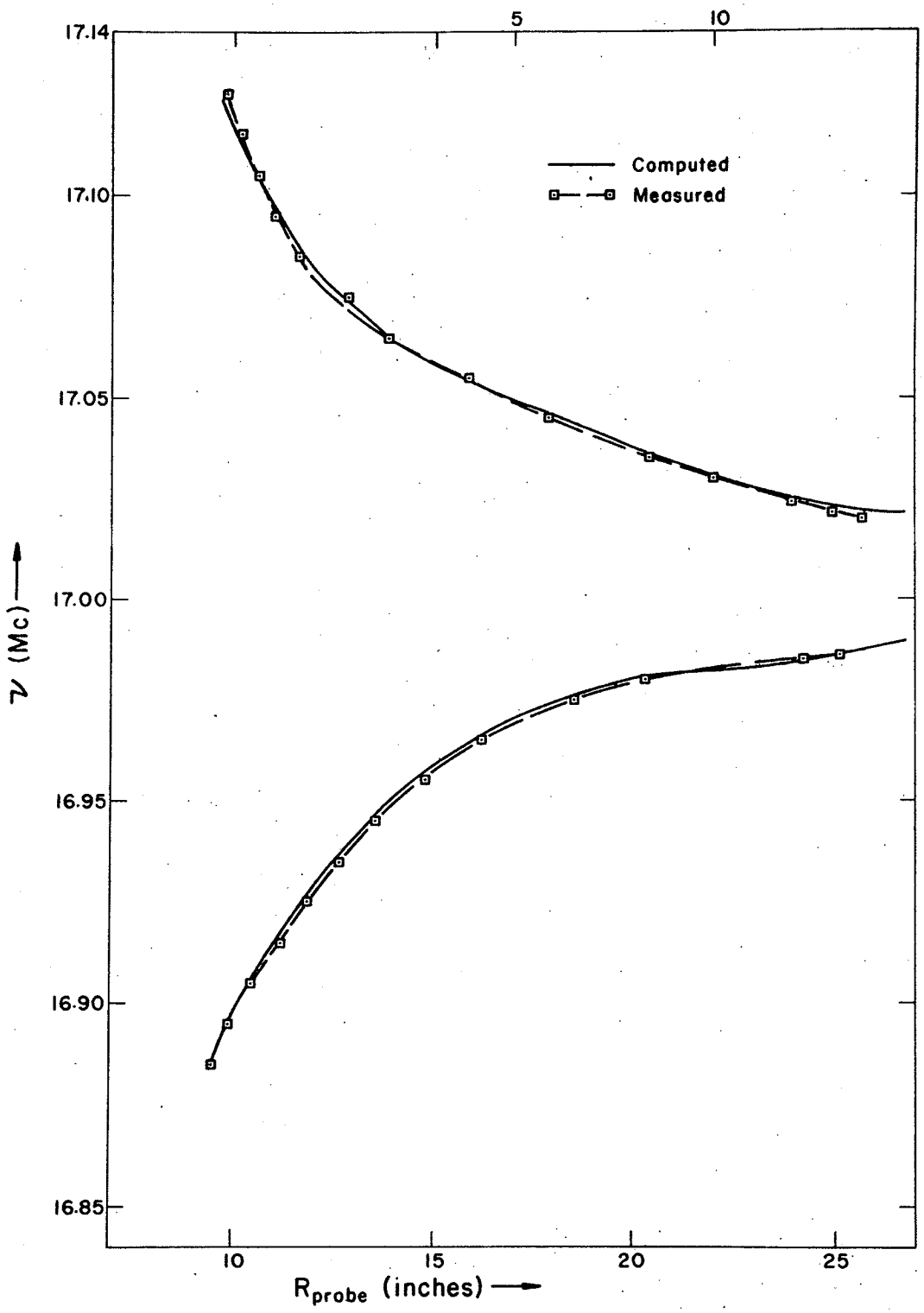

Figure 24. Envelope of frequency versus radius required to drive beam to half amplitude ($\sin\phi = \pm 1$ for central ray). Computed values obtained from SETOP are shown along with measured data for Field 200 (25 MeV protons).

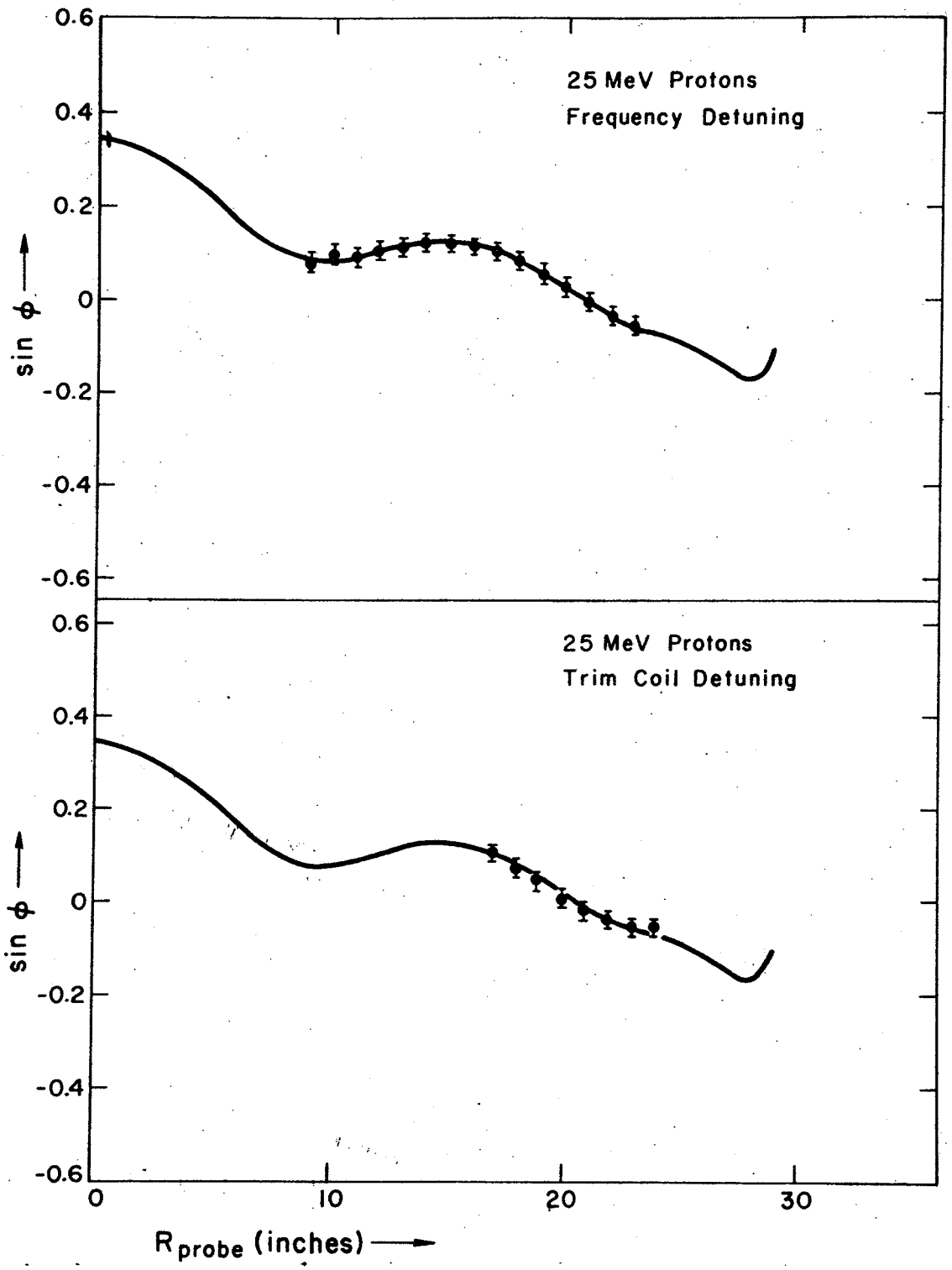

Figure 25. Sinϕ vs. probe radius for the 25 MeV proton field. Experimental data, obtained by frequency detuning and trim coil detuning, respectively, are compared to computed data obtained from SETOP.

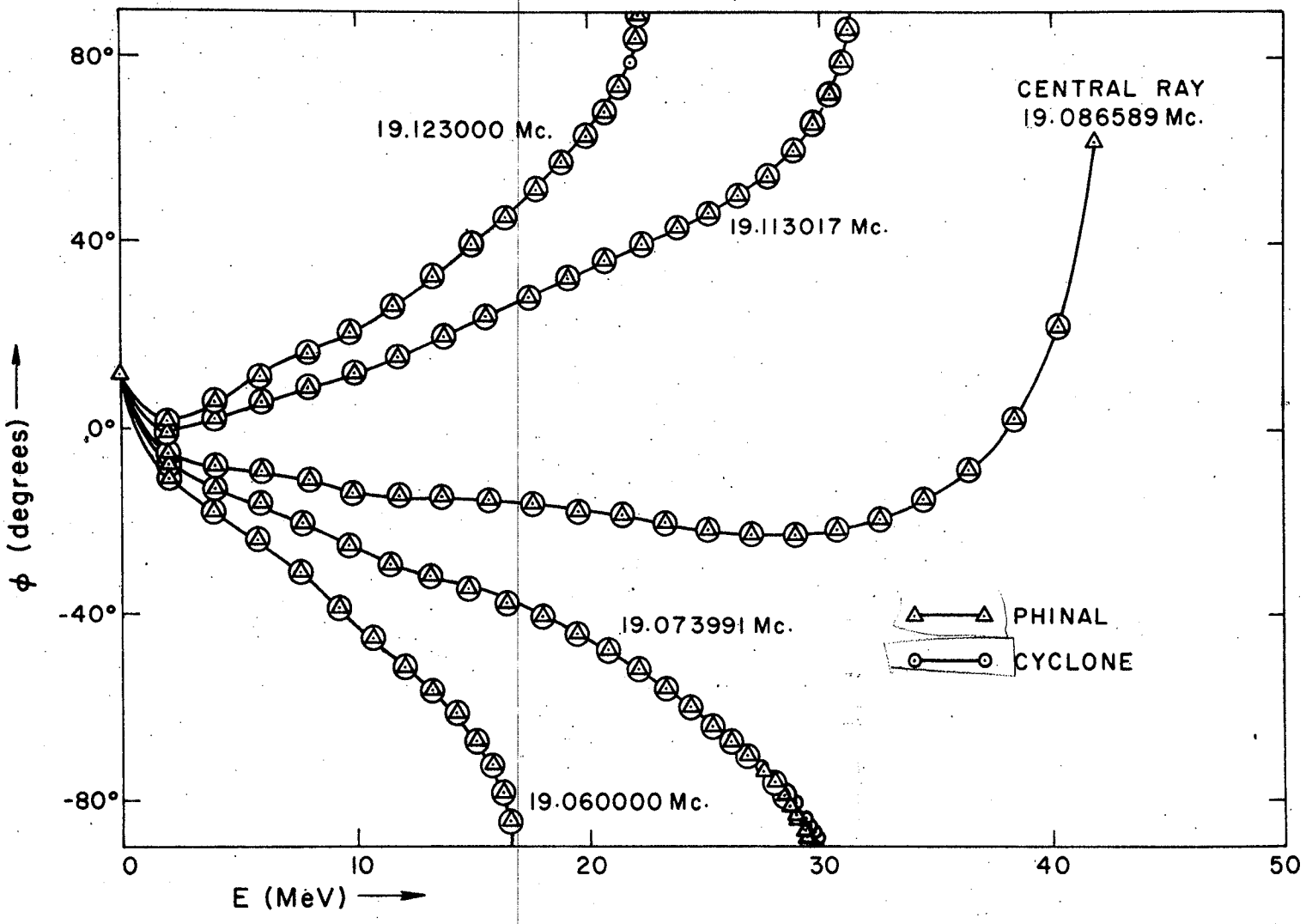

Figure 27. Comparison of sinφ vs. E for a 42 MeV field using a) the separated longitudinal equations as given in SETOP (PHINAL) and b) exact integration of the median plane equations of motion.

$$\sin\phi(E) = \sin\phi_o + \frac{2\pi h}{E_1} \int_o^E \left[\frac{B_o - \langle B\rangle}{\langle B\rangle}\right] dE \ , \qquad (8\text{-}8)$$

where B_o is the isochronous average field.

Since in this case it is more convenient to work directly with radius than energy, the relation:

$$E = \frac{p^2}{2m} = \frac{q^2 \langle B\rangle^2 R^2}{2m} \ , \qquad (8\text{-}9)$$

may be used to convert to a radial integral, with the final result:

$$\sin\phi(R) = \sin\phi_o + \frac{2\pi h q \omega_o}{E_1} \int_o^R [B_o - \langle B\rangle] R dR \ . \qquad (8\text{-}10)$$

Thus, introduction of deviations in the average field B(r) from the isochronous average field $B_o(r)$ results in deviations in the sine of the phase which are proportional to the weighted integral of the field differences. The derivation given above is not rigorous; however, the result is valid for small (first-order) field deviations—relativistic effects actually cancel out and flutter effects can be minimized by taking R as the mean radius of the equilibrium orbit.

If this equation is written twice, where in one of these the field of a trim coil is introduced specifically, subtracting the two equations yields:

tion (8-11) then contains the difference between two trim coil field functions in the integral. However, since the trim coil fields are assumed to be linear with respect to current, the ratio of the currents in the trim coils required to produce zero net field at the position of the slit remains constant, and equation (8-13) remains valid, where I_+ and I_- refer to the currents in the outer trim coil.

Because it is necessary to use two coils in combination to maintain the field at a constant value at the slit position, the possibility of introducing additional resonances must be considered. In the trim coil detuning measurements thus far carried out on the MSU cyclotron, trim coils number eight and two have been used with their ratio always set to maintain the central field undisturbed. (See Figs. 5 and 6.) The resulting error field possesses large gradients in the edge region of the inner coil; this can lengthen the radial extent of the $\nu_r = 1$ resonance and thereby introduce large radial oscillations into an otherwise stable beam, or if the gradient is large, a region of axial instability can result.

The importance of such phenomena was investigated by calculating equilibrium orbits in various displaced fields using trim coil currents computed to drive the beam to $\pm 90^\circ$ phase limits at various radii. Figure 28 shows the radial focusing frequency ν_r as a function of radius for a widely varied set of such displaced magnetic fields, including the

undisplaced field; Fig. 29 shows the axial focusing frequency ν_z as a function of radius for the same fields. (The field used here is the same 42 MeV proton field discussed previously.) The general absence of unstable conditions indicates that resonance errors are unlikely.

Another source of error can arise if magnetic field changes lead to variation of energy with radius. The equilibrium orbit data show only small variations in radius versus energy for field displacements which drive the beam off resonance at about half of the extraction radius. In addition, centering errors described previously can create inaccuracies in resulting measurements. These problems were investigated by computation of accelerated orbits in CYCLONE; a table of radius versus energy for several displaced fields is given in Table 3. Using appropriate starting conditions, the amplitude of the radial oscillation was retained at the minimal value of about one millimeter, and no increase of oscillation amplitude was observed with variation of trim coil current. The uniformity of the radius versus energy function indicates that no errors result from the use of the method of trim coil detuning.

A result of the theory, analogous to the case of frequency adjustment, is linearity of $\sin\phi$ with trim coil current. Examination of computed accelerated orbits verified this assumption to essentially the same degree as in the case of frequency variation. The linearity of $\sin\phi$ with

Table 3. Energy versus radius as a function of trim coil current for the 42 MeV field; such data establish the uniqueness of the radius as a function of energy within limits of experimental measurement, and validate the method of trim coil detuning described.

	ΔI_{TC8}=-33.80amps	ΔI_{TC8}=-22.49amps	ΔI_{TC8}=0	ΔI_{TC8}=+13.63amps	ΔI_{TC8}=+15.24amps
E	$\phi \rightarrow$ +90° at 24"	$\phi \rightarrow$ +90° at 27"	central ray	$\phi \rightarrow$ -90° at 27"	$\phi \rightarrow$ -90° at 24"
(MeV)	R(inches)	R(inches)	R(inches)	R(inches)	R(inches)
10	13.521	13.520	13.523	13.518	13.519
15	16.480	16.474	16.463	16.464	16.455
20	18.883	18.911	18.876	18.882	18.891
25	21.041	21.051	21.046	21.042	21.016
30	———	23.032	23.026	———	———

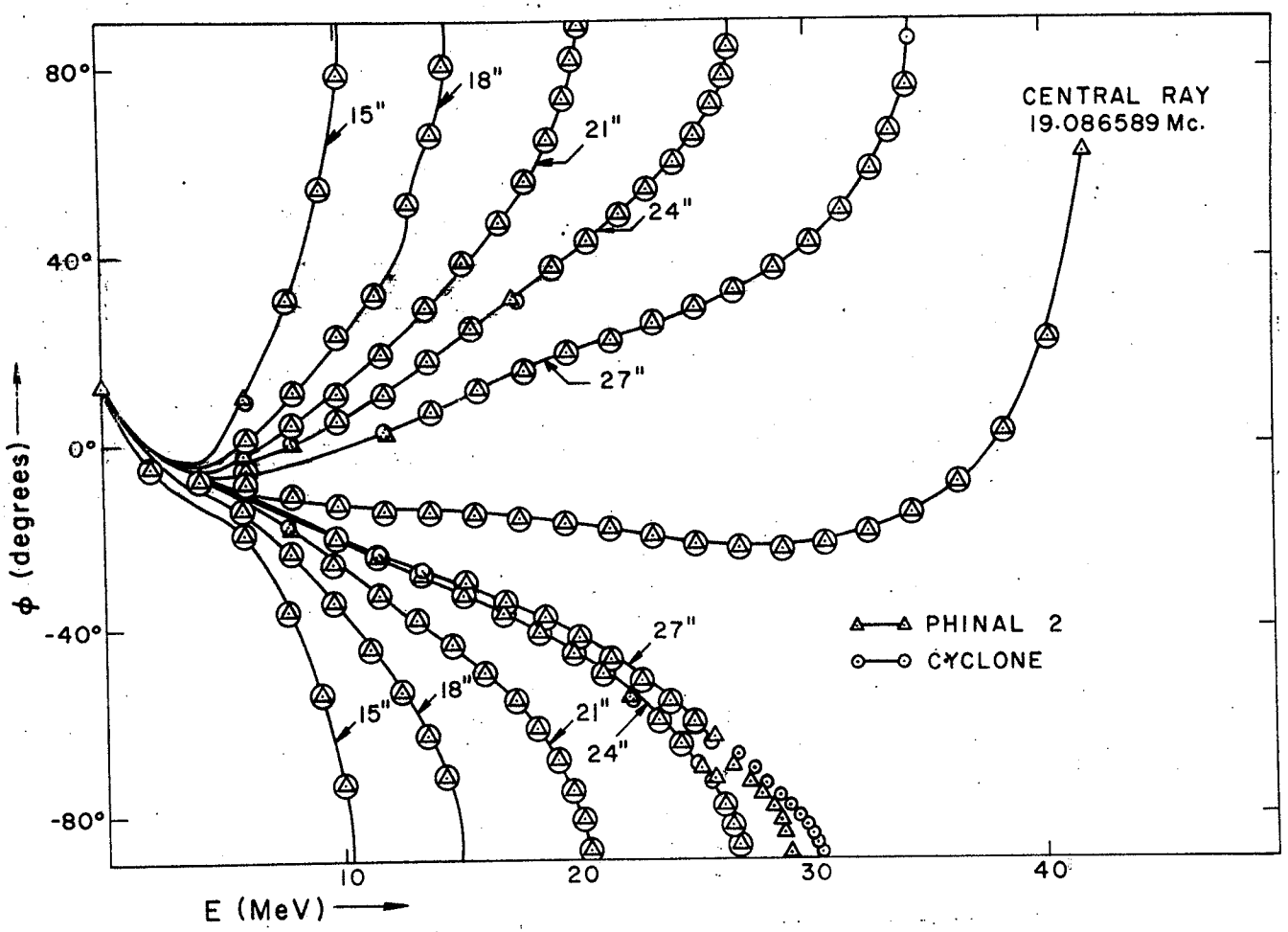

Figure 30. Comparison of sinφ vs. E obtained from a) integration of exact radial equations of motion (CYCLONE) and b) use of separated longitudinal equations in SETOP (PHINAL 2), for sets of detuned trim coil currents computed by the approximate relations used in SETOP to drive the central ray of the beam to ± 90° at several radii. The data for the 42 MeV proton field are illustrated.

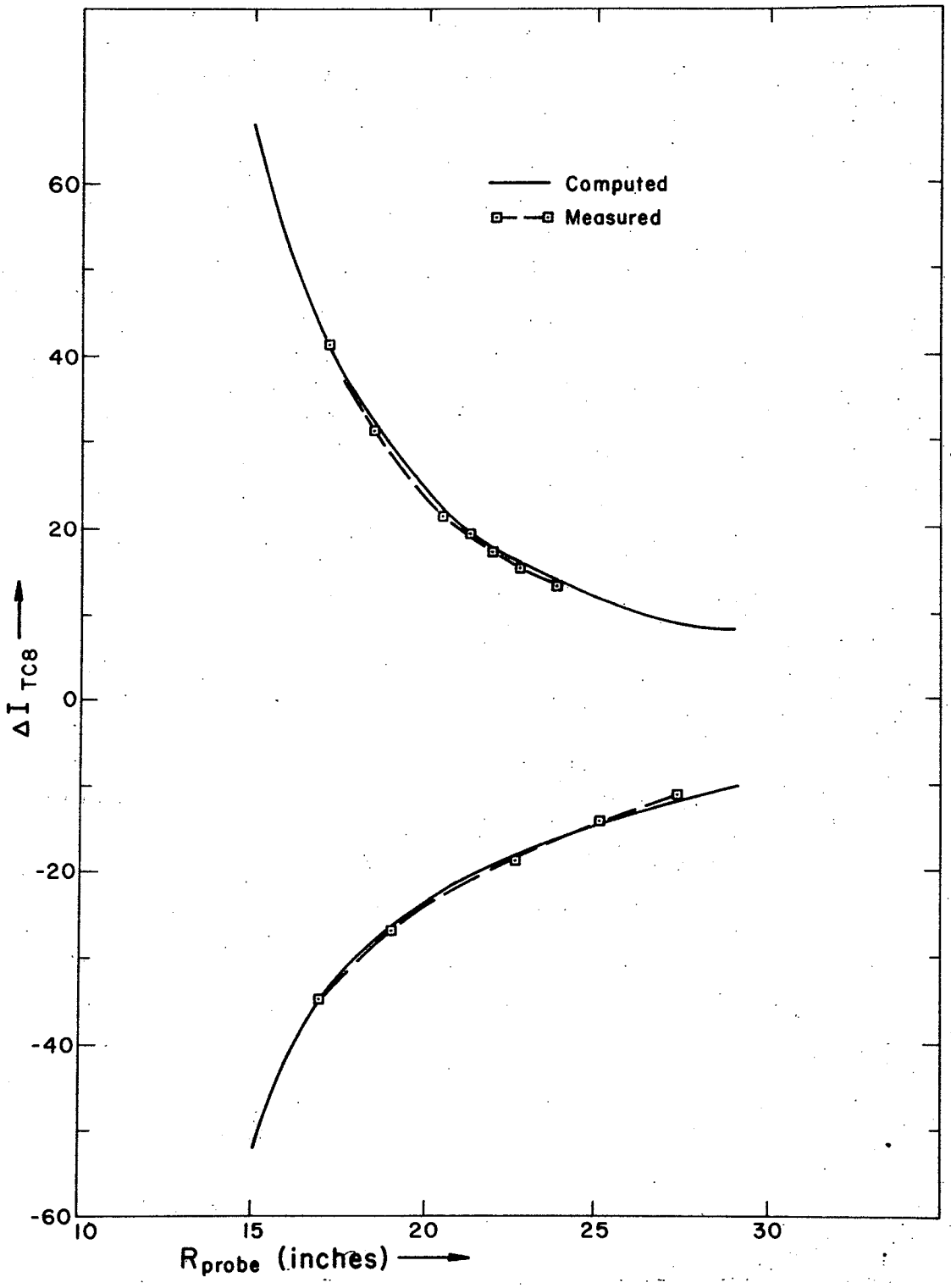

Figure 31. Envelope of trim coil 8 currents required to drive the central ray of the beam to ± 90° for the 25 MeV proton field (Run 200). Computed values obtained from SETOP are shown along with measured data.

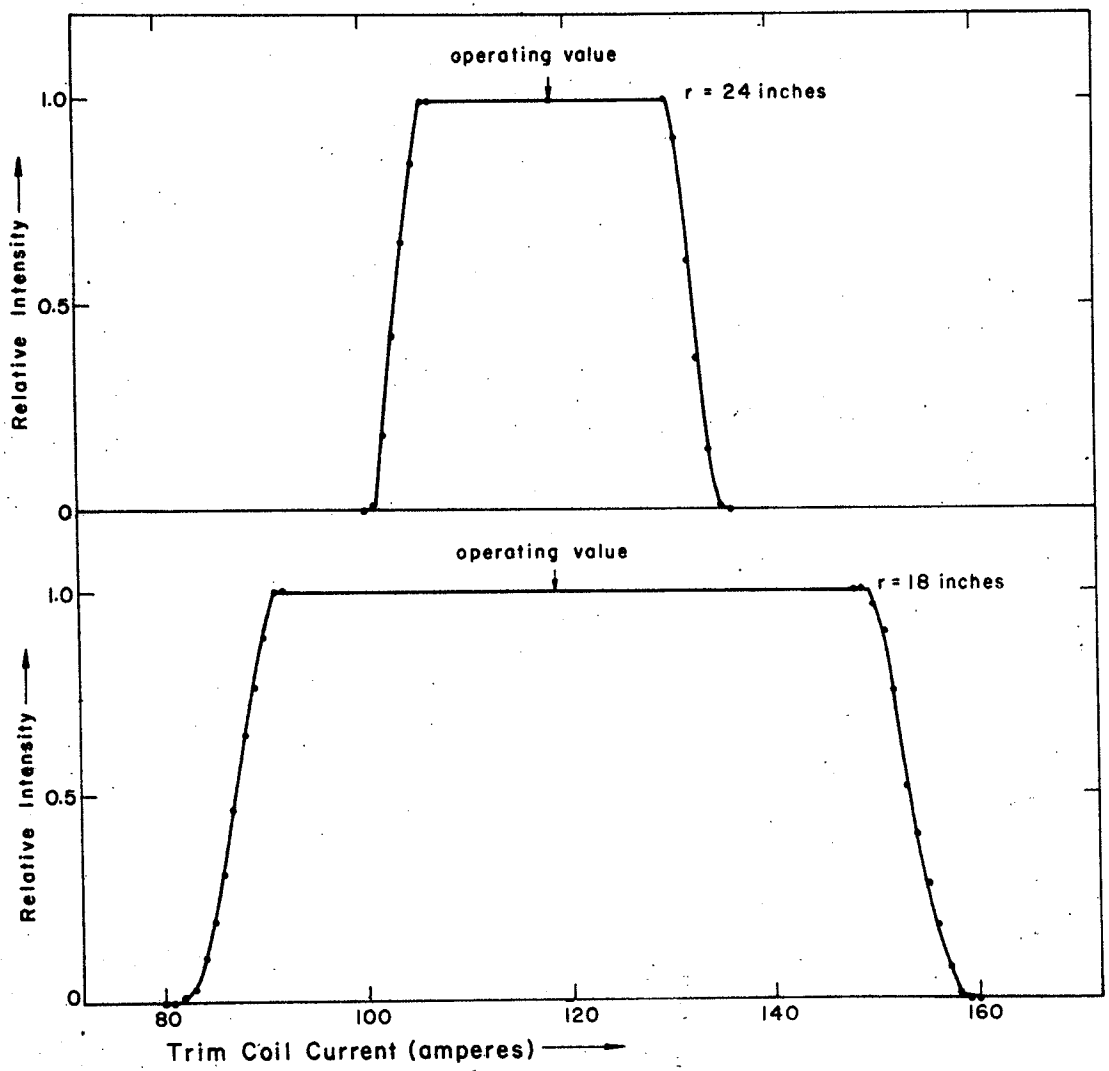

Figure 32. Beam intensity versus trim coil current at two radii in the 25 MeV proton field. These data can be used to obtain the central phase of the beam as a function of radius as well as the phase width of the beam.

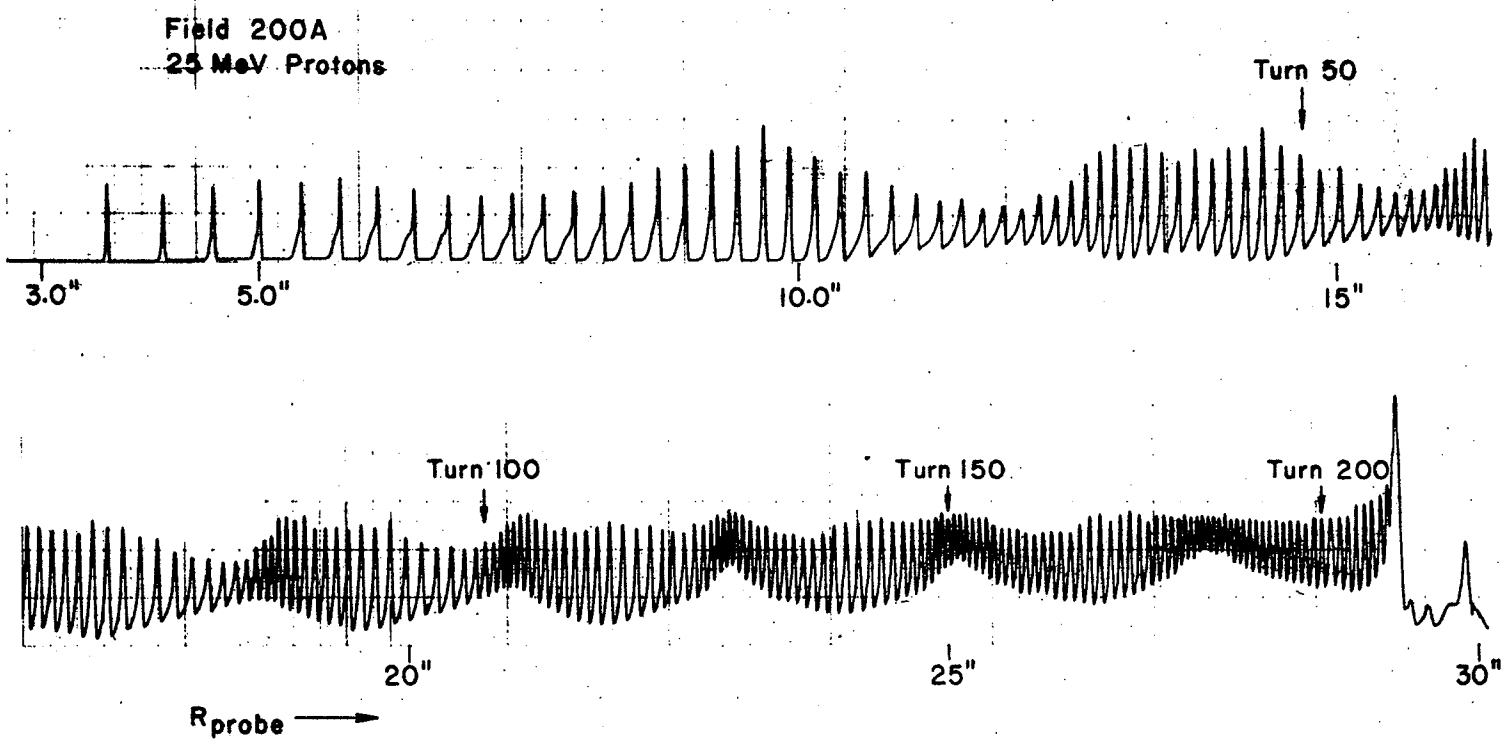

Figure 33. Radial differential probe pattern for 25 MeV protons.

high-radius side resulting from the parabolic radial contour of the turns appears in both plots. This striking agreement between the computed and measured patterns confirms the high quality of the calculations performed in obtaining the operating point, and the accuracy with which CYCLONE computes accelerated orbits in actual cyclotron fields.

8.5 Dee Voltage

Equations (8-4a) and (8-4b) may be solved to obtain the maximum energy gain per turn E_1 as a function of radius, in terms of the measured frequencies ω_+ and ω_-:

$$E_1 = \frac{\pi(\omega_+ - \omega_-)}{\omega_o} [E+F(E)] \qquad (8-14)$$

where the dee voltage is a function of E_1 depending upon the RF mode. (See Section 6-3.) The radial dependence of the dee voltage obtained in this manner is given in Fig. 35 for the 25 MeV, 33 MeV, and 42 MeV proton fields. These data are in good agreement with results of calculations in which the dees are composed of short sections of transmission line. It should be noted that E_1 cannot be obtained without reference to the calculations; the energy E and F(E) at each radius must be obtained by inspection of equilibrium orbit data.

8.6 Radial Focusing Frequency

It can be seen from Fig. 33 that the radial turn structure pattern possesses a periodic behavior; the radial focusing frequency is related to the number of turns in one precession cycle:

$$N_r = \frac{1}{|\nu_r - 1|} \quad . \tag{8-15}$$

The number of turns per cycle can be readily obtained from a turn structure pattern such as that of Fig. 33, and accurate experimental values for ν_r as a function of radius obtained. Figure 36 shows the computed ν_r versus radius curve for four magnetic fields, along with the experimental values obtained in the prescribed manner. The horizontal bars indicate the radial interval over which the turns were counted to obtain an average value of ν_r, and the vertical bars indicate the error in the average ν_r arising from inaccuracies in the number of turns counted. Note that for fields 200 and 300 both trim coil fields and main magnetic fields were measured. For field 250 the trim coil fields were obtained by interpolation, and field 280 was obtained entirely by interpolation in main magnet and trim coil fields.

8.7 Axial Focusing Frequency

A z-probe with a 1/8 inch square sensitive area which can be moved vertically over a 3/4 inch distance has been used to obtain data on axial motion. For these measurements

a large coherent axial oscillation was induced in the beam using a thin slit 0.15 inches above the median plane at the position of the first quarter turn. Making successive radial scans with the probe at various z-values, an effective nine-finger axial probe was obtained. Analyzing such data, it is possible to follow the coherent axial oscillation out to the edge region of the magnetic field. The number of turns in a complete cycle of axial motion is related to the focusing frequency:

$$N_z = \frac{1}{\nu_z} \quad . \tag{8-16}$$

Following the oscillation, the number of turns per cycle can be accurately obtained, allowing precise determination of ν_z. The results of such measurements are shown in Fig. 37 for the same fields shown in Fig. 36 to illustrate radial focusing frequency. The radial interval over which each average value of ν_z was obtained is indicated by the horizontal bars; the vertical error bars arise from errors in counting the number of turns per cycle of axial motion.

8.8 Summary

The excellent agreement between the beam properties obtained through computation and properties obtained experimentally verifies both the high quality of the magnetic field measurements and the accuracy of the SETOP computations performed in obtaining operating points. The precise agreement between computed and experimental properties clearly

demonstrates the power of the computer in predicting detailed behavior of orbits in cyclotrons.

10. A. A. Garren, Nuclear Instruments and Methods 18, 19 (1962), 309-322.

11. H. G. Blosser, M. M. Gordon, and T. I. Arnette, Nuclear Instruments and Methods 18, 19 (1962), 488-519.

12. H. G. Blosser and M. M. Gordon, Nuclear Instruments and Methods 13 (1961),101-117.

13. R. E. Berg, H. G. Blosser, and W. P. Johnson, Michigan State University Cyclotron Project Report MSUCP-22, August, 1966.

14. J. A. Futhey, Michigan State University Cyclotron Project Report MSUCP-18, July, 1963.

15. D. A. Lind, M. E. Rickey, and B. M. Bardin, Nuclear Instruments and Methods 18, 19 (1962), 129-134.

16. K. R. Symon, D. W. Kerst, L. W. Jones, L. J. Laslett, and K. M. Terwilliger, Physical Review 103 (1956), 1837-1859.

17. J. E. Stover, Michigan State University Cyclotron Project Report MSUCP-3, August, 1960.

18. H. G. Blosser, M. M. Gordon, and M. Reiser, Central-Region Studies for the MSU Cyclotron, Proceedings of the International Conference on Sector-Focused Cyclotrons and Meson Factories, CERN, April, 1962.

19. M. M. Gordon and D. A. Johnson, private communication.

20. M. M. Gordon and T. A. Welton, Computational Methods for AVF Cyclotron Design Studies, ORNL-2765.